Lysosomal cystine export regulates mTORC1 signaling to guide kidney epithelial cell fate specialization

Marine Berquez[1,*], Zhiyong Chen [1,*], Beatrice Paola Festa[1,*], Patrick Krohn[1],

Svenja Aline Keller[1], Silvia Parolo[3], Endre Laczko[4], Enrico Domenici[3,5],

Olivier Devuyst[1,6,#] and Alessandro Luciani[1,#]

[1]Institute of Physiology, University of Zurich, 8057 Zurich, Switzerland;

[2]Division of Clinical Chemistry and Biochemistry, University Children's Hospital Zurich, CH–8032 Zurich, Switzerland;

[3]Fondazione The Microsoft Research University of Trento, Centre for Computational and Systems Biology (COSBI), 38068 Rovereto, Italy;

[4]Functional Genomics Center Zurich, University of Zurich, Winterthurerstrasse 190, CH–8057, Zurich, Switzerland.

[5]Department of Cellular, Computational and Integrative Biology (CIBIO), University of Trento, 38123 Trento, Italy;

[6]Institute for Rare Diseases, UC Louvain Medical School, 1200 Brussels, Belgium.

[*]MB, ZC, and BPF contributed equally; [#]OD and AL co-directed the study

Correspondence: olivier.devuyst@uzh.ch (O.D.) or alessandro.luciani@uzh.ch (A.L.)

Abstract

Differentiation is critical for epithelial cell fate decisions, but the signals involved remain unclear. The kidney proximal tubule (PT) cells reabsorb disulphide-rich proteins through endocytosis, generating cystine via lysosomal proteolysis. Here we report that defective cystine mobilization from lysosomes through cystinosin (CTNS), which is mutated in cystinosis, diverts differentiation of PT cells towards growth and proliferation, disrupting their functions. Mechanistically, lysosomal cystine storage stimulates Ragulator-Rag GTPase-dependent recruitment of mTORC1 and its constitutive activation. Re-introduction of CTNS restores nutrient-dependent regulation of mTORC1 in knockout cells, whereas cell-permeant analogues of L-cystine, accumulating within lysosomes, render wild-type cells resistant to nutrient withdrawal. Therapeutic mTORC1 inhibition corrects lysosome and differentiation downstream of cystine storage, and phenotypes in a zebrafish model of cystinosis. Thus, cystine serves as a lysosomal signal that tailors mTORC1 signaling and metabolism to direct epithelial cell fate decisions. These results identify mechanisms and therapeutic targets for dysregulated homeostasis in cystinosis.

Introduction

The epithelial cells lining the kidney proximal tubule (PT) play a critical role in homeostasis by efficiently reabsorbing small proteins from the primary urine. The process is mediated by receptor-mediated endocytosis and lysosomal pathways, preventing the loss of precious nutrients in the urine (1). The lysosomal degradation of disulphide-rich plasma proteins like albumin accounts for the supply of cystine that is exported to cytoplasm through the lysosomal cystine transporter cystinosin (CTNS; ref. 2). In the cytoplasm, cystine is reduced to cysteine and utilized for the maintenance of cellular redox homeostasis (3). Additionally, the lysosome-mediated removal of dysfunctional mitochondria regulates the differentiating state of PT cells through junctional integrity and transcriptional programs, including the transcription factor Y box 3 (Ybx3) (4). Recessive mutations in *CTNS*, the gene that encodes cystinosin (CTNS), cause cystinosis, a lysosomal storage disease characterized by loss of endocytosis/reabsorptive properties of PT cells, progressing towards kidney failure (5). How, mechanistically, the increased levels of cystine within lysosomes, reflecting its defective export through CTNS, affect fate decisions remains unknown.

A crucial step in nutrient sensing is the recruitment of the evolutionarily conserved mTORC1 to lysosomes (6). In presence of nutrients, such as amino acids, glucose, and lipids, a multiprotein complex composed of Rag guanosine triphosphatases (Rag GTPases), Ragulator, and vacuolar H^+-ATPase (V–ATPase) tethers mTORC1 to the lysosomal surface, enabling its activation by the growth factor-induced GTPase Rheb (7,8). Signaling from lysosomes, mTORC1 signaling promotes growth and proliferation while repressing lysosome biogenesis and catabolic autophagy (9). The proper regulation of mTORC1 signaling sustains polarized transport properties in epithelial cell types (10). This has been well illustrated in the kidney, where hypo and/or hyperactivation of mTORC1 pathway can drive pathological changes in podocytes and tubular cells, whereas blunting of hyperactive mTORC1 may prove beneficial in renal cell carcinoma and polycystic and/or diabetic kidney disease (11).

Like other lysosomal amino acid transporters, the CTNS protein physically interacts with V-ATPase-Ragulator-Rag GTPase lysosomal scaffold that activates mTORC1 (12). During periods of starvation in *Drosophila*, mobilization of cystine from lysosomes fuels acetyl-CoA synthesis and limits TORC1 reactivation, altogether balancing catabolic autophagy and growth in developing organisms (13). In the mammalian kidney, PT cells are particularly vulnerable to imbalances in metabolism, which can curb their differentiation and cause disease (14). These findings raise the possibility that lysosomal cystine export may shape the response of mTORC1 and metabolism to fate decisions during the differentiation of the kidney tubule epithelium.

Here, we combine genetic model organisms (mouse, rat, and zebrafish) and physiologically relevant cell culture systems to test the causal role of an evolutionarily conserved pathway that tunes mTORC1 signaling and metabolism in response to levels of lysosomal cystine to instruct fate specialization. Together the results provide insights into the mechanisms that regulate homeostasis and specialized function in kidney epithelial cells, and therapeutic targets for cystinosis.

Results

Cystine storage and defective lysosomes divert differentiation towards proliferation

The genetic deletion of *Ctns* in mouse induces cystine storage and lysosome abnormalities in the kidney PT (Fig. 1a,b), leading to defective receptor-mediated endocytosis of low molecular weight proteins (LMWPs; Fig.1c) and their losses in the urine (Fig. 1d). Genome-wide transcriptional profiling of PT segments from *Ctns* knockout (KO) versus wild-type (WT) littermates (Fig.1e; Supplementary Fig. 1a) identified 61 genes differentially expressed between *Ctns*^{KO} and *Ctns*^{WT} PT segments, of which 43 were upregulated and 18 downregulated, respectively (Supplementary Table 1). Gene set enrichment pathway analysis (GSEA) revealed a striking upregulation of cell cycle, whereas membrane trafficking and vesicle-mediated/small molecule transport, and hemostasis were significantly downregulated (Fig. 1f). The dysregulation of genes related to these pathways was verified (Supplementary Fig. 1b), with increased levels of proteins regulating cell cycle (Ccna2 and Cdc20) and proliferation (Pcna), contrasting with decreased levels of the multiligand receptor Lrp2/megalin, the master coordinator of LMWP uptake (15), in the PT of *Ctns*^{KO} kidneys compared to *Ctns*^{WT} littermates (Fig. 1g,h; Supplementary Fig. 1c,d).

Since *Ctns* associates with lysosomes (Supplementary Fig. 2a-b), we next investigated whether changes in growth/proliferation induced by CTNS loss/cystine storage reflect alterations in lysosomal catabolic activities, using primary cells derived from microdissected PT segments (referred to as mPTCs; Ref. 4) of mouse *Ctns* kidneys. The *Ctns*^{KO} mPTCs, which accumulate cystine within lysosomes (Supplementary Fig. 2c) and show abnormal growth/proliferation rates and defective endocytosis of fluorescent-tagged ligands (Fig. 1i,j) mimicking the changes observed *in vivo*, displayed reduced numbers of functionally degradative lysosomes, both under full and nutrient-depleted conditions, compared to *Ctns*^{WT} cells (Supplementary Fig. 2d-f). In agreement, *Ctns*^{KO} cells showed higher numbers of Map1lc3b-positive autophagic puncta and autolysosomes, insensitive to treatment with BfnA1 for different time points (Fig. 1k; Supplementary Fig. 2g). Comparative analysis of lysosome proteins from *Ctns*^{KO} versus *Ctns*^{WT} mPTCs transiently expressing the lysosomal

membrane protein Tmem192 fused to 3×haemagglutinin (T192-3×HA; Supplementary Fig. 3a-f) revealed decreased proteolytic generation of the 32 kDa luminal mature CtsD and augmented levels of the lipidated, autophagosome-associated form Map1Lc3b-II (Fig. 1l). Similar alterations were also observed in the *Ctns*^{KO} kidneys (Supplementary Fig. 3g). Thus, cystine build-up secondary to the loss of CTNS rewires the metabolism from catabolic programs towards growth/proliferation, disrupting the differentiating state of PT cells and their endocytosis/reabsorptive properties.

Hyperactive mTORC1 signalosome drives the metabolic switch

To identify the factors that drive the metabolic switch induced by CTNS loss/cystine storage, we conducted proteomics- and metabolomics-based profiling of *Ctns* mPTCs (Fig. 2a). PCA and hierarchical clustering revealed that proteome and metabolome of *Ctns*^{KO} mPTCs substantially differ from the *Ctns*^{WT} control cells (Fig. 2b,c; Supplementary Fig. 4a-b). Protein-protein interaction analysis of differentially expressed proteins revealed significant enrichment in metabolism, cell cycle and ribosome biogenesis, growth and proliferation, apoptosis regulation, signal transduction, and differentiation pathways in *Ctns*^{KO} versus *Ctns*^{WT} mPTCs (Supplementary Fig. 4c,d). Metabolite set enrichment analysis (MSEA) identified in *Ctns*^{KO} cells chemical categories predominantly containing amino acids, organic acids, sugars, and nucleotides (Supplementary Fig. 4e,f). In particular, the amino acid metabolism (alanine, arginine, and glycine and serine), glycolysis and gluconeogenesis (thiamine, malate-aspartate, biotin, and pyruvaldehyde), fatty acid synthesis (biotin and pyruvaldehyde), urea cycle (phenylacetate and urea), and glutathione synthesis were enriched in *Ctns*^{KO} versus *Ctns*^{WT} mPTCs (Supplementary Fig. 4g). Integrated biological network analysis crossing differentially produced proteins with metabolites (Fig. 2b,c; Supplementary Table 2) identified in *Ctns*^{KO} mPTCs an enrichment of pathways linked to regulation of the mTORC1 signalosome, such as glucose and amino acids (6), mTORC1 signaling itself, and downstream anabolic (protein, fatty acid, and nucleotide biosynthesis) or catabolic (autophagy) processes. An enrichment in pathways related to cancer cell

metabolism and renal cell carcinoma, known to be driven by aberrant mTORC1 signaling (16), was also observed (Fig. 2d).

We next examined the mTORC1 signaling in CTNS-deficient PT cells. The CTNS loss rendered mTORC1 less sensitive to nutrient starvation and constitutively active, as indicated by persistent phosphorylation of the ribosomal protein S6 ($pS6^{Ser235/236}$) and eukaryotic translation initiation factor 4E (eIF4E)-binding protein 1 ($p4EBP1^{Ser65}$) (Fig. 2e). Increased phosphorylation rates of the canonical mTORC1 substrate ($pS6^{Ser235/236}$) were also observed in *Ctns*^{KO} kidneys (Supplementary Fig. 5a,b). In agreement, CTNS loss/cystine storage augmented the lysosomal protein levels of components (17) of V-ATPase subunit Atp6v0d1, Ragulator complex subunit Lamtor2 and RagC that control mTORC1 activation (Fig. 2f). In *Ctns*^{KO} mPTCs, RagC was strongly clustered on Lamp1-positive structures compared to *Ctns*^{WT} mPTCs (Fig. 2g), substantiating the regulatory effect of CTNS on mTORC1 activation.

The impact of CTNS loss on mTORC1 signaling was further examined in *ctns*-deficient zebrafish (4) and *Ctns*^{KO} rat model (18), both displaying significant cystine storage, metabolic defects, and PT cell dedifferentiation (Supplementary Fig. 5c-f). Increased phosphorylation rates of $pS6^{Ser235/236}$ in the kidney PT of *Ctns*^{KO} rat and in *ctns*-deficient zebrafish compared to their respective controls (Fig.2h-j) demonstrated the evolutionary conservation of this connection.

Temporal mTORC1 activation by cystine storage directs kidney disease development

The possibility to monitor progressive PT dysfunction (Fig. 3a) and cystine storage (Fig. 3b) over time allowed us to test whether mTORC1 activation may drive the onset and progression of kidney disease in CTNS deficient mice (Fig.3c). Analyses in mPTCs from *Ctns*^{KO} kidneys revealed nutrient-dependent mTORC1 activation, similar to control *Ctns*^{WT} mPTCs, at 6 weeks of age (Fig. 3d). Conversely, in mPTCs from pre-symptomatic 12-week-old *Ctns*^{KO} mice, mTORC1 activation was stronger than in control cells and largely resistant

to nutrient starvation (Fig. 3e). Like wild-type cells, mTOR translocated to the surface of Lamp1-flagged lysosomes in presence of nutrients in mPTCs from 6-week-old *Ctns*^{KO} kidneys, but it readily dissociated from lysosomes following nutrient starvation (Fig. 3f), as expected in response to changes in nutrient availability. Conversely, in mPTCs from 12-week-old *Ctns*^{KO} kidneys, mTOR remained clustered on Lamp1-flagged lysosomes following nutrient deprivation, contrasting with the dissociation observed in control cells (Fig. 3g). These changes were accompanied by reduced numbers of enlarged Lamp1^{+} structures in mPTCs from kidneys of 6- to 12-week-old *Ctns*^{KO} mice (Supplementary Fig. 6a). The effect of CTNS loss/cystine storage on mTORC1 activity did not result from alterations in growth factor-directed or AMPK-mediated signaling upstream of mTORC1, which were similar between wild-type and *Ctns*^{KO} mPTCs (Supplementary Fig. 6b). Thus, CTNS loss/ cystine storage activates mTORC1 through mechanisms that are, at least in part, distinct from growth factor-induced signals and/or energy availability.

Lysosomal cystine regulates mTORC1 through Ragulator-Rag GTPase complex

We next tested whether cystine storage per se might force mTORC1 to remain on the lysosomal surface, using pharmacologic and genetic tools. Emptying the cystine stores with the drug cysteamine (19) blunted mTORC1 activation in mPTCs derived from 24-week-old *Ctns*^{KO} mice (Fig. 3h,i). Notably, the latter treatment corrected the mTORC1 activation to the same extent than the selective mTOR inhibitor Torin1 which, contrary to cysteamine, does not empty the cystine storage (Fig. 3h,i).

To substantiate the causal link between CTNS loss, lysosomal cystine storage, and hyperactive mTORC1 signaling, we transduced *Ctns*^{KO} PT cells with an adenovirus expressing HA-tagged wild-type (HA-CTNS^{WT}) or Gly339Arg mutant (HA–CTNS^{G339R}) CTNS (Fig. 4a; Supplementary Fig. 7a). This disease-causing CTNS^{Gly339Arg} mutant (20) preserves the delivery of the mutant CTNS to the lysosomal surface while abrogating its transport function and thus causing cystine storage (Fig. 4b; Supplementary Fig. 7b). The re-introduction of CTNS^{WT} in *Ctns*^{KO} mPTCs rescued the cystine levels (Fig. 4b) and restored

the nutrient-directed regulation of mTORC1 compared to *Ctns*^{KO} mPTCs transduced with an empty vector (Fig. 4c; +HA-CTNS^{WT}). Conversely, the nutrient-dependent regulation of mTORC1 signaling activity was markedly abolished in *Ctns*^{KO} mPTCs expressing mutant CTNS^{G339R}/ accumulating cystine (Fig. 4b), as evidenced by elevated phosphorylation rate of mTORC1 substrate S6 (Fig. 4c; +HA-CTNS^{G339R}) in nutrient–depleted conditions. Immunoblotting analyses of anti-HA immunoprecipitates from *Ctns*^{KO} mPTCs transiently expressing diverse tagged CTNS forms revealed a decreased binding of CTNS^{WT} to endogenous members of Ragulator-Rag GTPases lysosomal scaffold (e.g., Lamtor2 and RagC) compared to mPTCs transducing with mutant CTNS^{G339R} (Fig. 4d). In line, the reconstitution with CTNS^{WT}, but not the mutant CTNS^{G339R}, rescued autophagy-lysosome degradation systems in *Ctns*^{KO} mPTCs (Supplementary Fig. 7c,d).

To prove that lysosomal cystine is involved in this signaling loop, we bypassed the transport function of CTNS by culturing *Ctns*^{WT} mPTCs with cystine methyl ester derivates (CDME; 17,21). These amino acid derivates rapidly enter the cells and are hydrolysed by esterases into native amino acids, ultimately accumulating within mPTCs and lysosomes (Fig. 4e-g). Exposure of nutrient-depleted *Ctns*^{WT} mPTCs with low, non-toxic doses of CDME stimulated mTORC1 activity in a time-dependent fashion (Fig. 4h; Supplementary Fig. 7e-g). This lag correlated with the time required for CDME to accumulate within lysosomes and appeared to be highly specific because it could not be recapitulated by treating starved cells with unmodified L-cystine analogues that do not accumulate (Fig. 4f,g). Immunoblotting analyses of anti-HA immunoprecipitates from mPTCs transiently expressing tagged CTNS^{WT} revealed an increased binding of tagged CTNS to endogenous components of Ragulator-Rag GTPases lysosomal scaffold (e.g., Lamtor2 and RagC) in CDME-treated cells compared to those exposed to unmodified L-cystine analogues (Fig. 4i). Collectively, these data reveal that, through interactions with Ragulator-Rag GTPase lysosomal scaffold, CTNS regulates the activation of mTOR in response to variations in the levels of lysosomal cystine.

Blocking mTORC1 rescues lysosome proteolysis and cell differentiation downstream of cystine storage

We then used pharmacological and genetic tools to test whether mTORC1 inhibition restores lysosomal catabolic activities and differentiating state of PT cells lacking CTNS/accumulating cystine. We treated *Ctns*^{WT} and *Ctns*^{KO} mPTCs with low, non-toxic doses of Torin1 (250nM for 24 h; Supplementary Fig. 8a). Treatment with Torin 1, which fails to correct cystine storage (Fig.3j) while effectively blocking mTORC1 activity (Fig. 5a, Supplementary Fig. 8b), enhanced the nuclear translocation of the transcription factor E3 (Tfe3), the master modulator of lysosome biogenesis and autophagy (9), in *Ctns*^{KO} mPTCs compared to vehicle. In turn, the increased nuclear import heightened Tfe3-targeted autophagy and lysosomal genes, re-activating lysosome function and catabolic autophagy (Fig. 5b,c; Supplementary Fig. 8c-f). In agreement with the rescue of autophagy-lysosome degradation systems, treatment with Torin1 ameliorated the mitochondrial bioenergetics and lowered the overproduction of mitochondrial ROS, preventing the disruption of tight junctions manifested in *Ctns*^{KO} mPTCs (Fig. 5d,e; Supplementary Fig. 8g,h). This markedly repressed the nuclear translocation of Ybx3 and its driven activation of growth/proliferation (Fig. 5f-i), while resetting the differentiation and endocytic/reabsorptive functions of *Ctns*^{KO} PT cells (Fig. 5g,j).

Similar functional rescues, including lysosomal catabolic activities, autophagy, proliferation, and differentiation were also observed in *Ctns*^{KO} cells depleted of *Raptor* (Supplementary Fig. 9), a gene encoding protein that docks the mTOR protein kinase on the surface of lysosomes (6). Furthermore, treatment of *Ctns* rats with low doses (22) of the allosteric mTOR inhibitor Rapamycin (1.5 mg/kg/day for 2 weeks) reduced/normalized mTORC1 activity and lysosomal abnormalities (Supplementary Fig. 10a-c), and inhibited growth/proliferation while restoring Lrp2-mediated endocytosis in kidney PT cells lacking CTNS (Supplementary Fig. 10d,e) compared to those treating with vehicle. These phenotype rescues occurred in the absence of significant changes in rat kidney cystine levels (Supplementary Fig. 10f). Thus, genetic and pharmacological suppression of mTORC1

signaling corrects the lysosomal catabolic activities and differentiating/functional states of PT cells downstream of CTNS loss/ cystine storage.

mTORC1 inhibition improves PT dysfunction in a zebrafish model of cystinosis

Finally, to test whether mTORC1 inhibition rescues PT dysfunction *in vivo*, we treated *ctns* zebrafish expressing a bona fide LMW biosensor for PT function (lfabp10a::½ vdbp–mCherry; Fig. 6a; Ref. 23) with low, non–toxic doses of Rapamycin. Treatment with Rapamycin, which efficiently blunts mTORC1 activity (Fig. 6b), rescued PT function in *ctns*^{KO} zebrafish pronephros, as evidenced by substantial decreases in LMWP/mCherry levels in treated *ctns*^{KO} zebrafish compared to those receiving the vehicle (Fig. 6c). The phenotype rescues occurred without changes in cystine levels in *ctns*-deficient zebrafish (Supplementary Fig. 10g). Similarly, mTORC1 inhibition by low-doses of the biguanide drug metformin, the most prescribed glucose-lowering medication worldwide with potential benefits on nutrient sensing (24), significantly rescued PT function in *ctns*^{KO} zebrafish compared to those treated with vehicle (Fig. 6d,e). Taken together, these proof-of-concept studies indicate that modulation of mTORC1 signaling may serve as an attractive therapeutic strategy for treating PT dysfunction in cystinosis.

Discussion

Here, we demonstrate that cystine mobilization from lysosomes is crucial for maintaining the differentiation and endocytic function of PT cells. Lysosomal cystine storage, typically caused by the functional loss of CTNS, diverts the fate of PT cells towards growth/proliferation, disrupting their reabsorptive properties. Mechanistically, cystine storage stimulates Ragulator-Rag GTPase-dependent recruitment of mTORC1 and its constitutive activation. In cells and preclinical models, the modulation of mTORC1 pathway restores lysosome function and catabolic autophagy, ultimately steering the proliferative/growing states of PT cells towards differentiation, hence their physiological homeostasis (Supplementary Fig. 11).

Our findings show that lysosomes accumulating cystine due to CTNS loss display profound defects in their catabolic properties, with marked accumulation of intracellular constituents that are normally dismantled through autophagy (25). These anomalies are paralleled by the upregulation of programs for growth/proliferation while suppressing the differentiation of the PT cells, hence causing defective receptor-mediated endocytosis, i.e., the earliest manifestation of epithelial cell disease (5). How do CTNS-deficient/cystine accumulating lysosomes affect cell fate specialization and differentiation programs? Our integrative multi-omics analyses, combined with cross-species validation, indicate that lysosomal cystine storage constitutively activates mTORC1 signaling in CTNS-deficient PT cells. These findings are in line with previous studies showing hyperactive mTORC1 pathway in other lysosomal storage diseases characterized by the abnormal accumulation of intracellular metabolites, e.g., cholesterol in Niemann Pick type C (NPC) and glycosaminoglycans in Mucopolysaccharidosis type VII (9,26-28). Conversely, mTORC1 activity seems to be reduced/unchanged in transformed, proliferative tubular cells derived from cystinosis patients and in patient-derived iPSCs (12,29-30). Such discrepancies may be related to immortalization protocols, which reduce per se the phosphorylation rates of canonical mTORC1 substrates (31), or to use of dedifferentiated cellular systems that poorly recapitulate the physiological characteristics of native kidney tubular cells.

The mTORC1 hyperactivation evidenced in CTNS-deficient mPTCs and in the three model organisms, together with time-course of cystine accumulation and lysosomal mTORC1 dynamics, suggests that CTNS tailors the activation of mTORC1 signaling in response to lysosomal cystine levels. Treatment of CTNS-defective mPTCs with cysteamine, which facilitates the export of cystine from lysosomes through the cationic amino acid PQ-loop repeat-containing protein 2 (PQLC2; ref. 5), or the exposure of wild-type mPTCs to CDME, which accumulates within lysosomes independently of CTNS, reduces and stimulates, respectively, mTORC1 activation at the lysosomal surface. Re-introduction of $CTNS^{WT}$, which reinstates the lysosomal cystine efflux compared to disease-causing mutant $CTNS^{G339R}$, successfully restored the sensitivity of mTORC1 to changes in nutrient availability in CTNS-defective PT cells. Conversely, CDME-induced cystine storage within lysosomes of wild-type PT cells, rendered mTORC1 insensitive to nutrient withdrawal. In both contexts, variations in the levels of lysosomal cystine appear to modulate mTORC1 activation through the binding of CTNS with components of Rag GTPase-Ragulator lysosomal scaffold. In agreement, CTNS-deficient lysosomes displayed increases in the levels of RagC, V-ATPase subunit Atp6v0d1, and Lamtor2 proteins. Like in cells lacking the lysosomal cholesterol transporter NPC1 where cholesterol storage drives mTORC1 activation through association with the lysosomal transmembrane protein, SLC38A9 (26), the elevated levels of lysosomal cystine may affect the mTORC1 activating machinery through the combined action of a yet-undefined positive regulator and a negative modulator, the CTNS protein.

Alternatively, CTNS may function as a transceptor (e.g., transporter with a receptor-like function) involved not only in the mere transport of cystine but also in which the amino acid engagement is used for allosteric signal transduction (32), as recently described for other nutrient transporter systems (33), including the human solute transporter SLC38A9 (34). Interestingly, the binding of arginine to SLC38A9 seems to release a short β hairpin/plug that can act as a receptor to signal the activation of Ragulator-Rag GTPase

scaffold and therefore of mTORC1 (35,36). The existence of plug-and-socket mechanisms in nutrient signaling by CTNS merits further structural analyses and biochemical validation.

Our study offers therapeutic targets to rewire homeostasis in cystinosis, a life-threatening disease for which cysteamine has remained the standard of care, despite major side-effects (5,19). In view of the hyperactive mTORC1 signaling and disturbed homeostasis in diseased *Ctns*^{KO} kidneys, its inhibition may enhance Tfe3-mediated re-activation of cellular programs boosting lysosomes and catabolic autophagy, with the removal of damaged (ROS-overproducing) mitochondria, stabilization of the tight junctions, and repression of the Ybx3 signaling cascade that promotes dedifferentiation and growth/proliferation downstream of cystine accumulation. However, the translatability of mTORC1 inhibitors is limited by poor availability, lack of specificity, and toxicity (6). The proof-of-principle rescue of cellular and functional defects observed with the use of rapamycin (37) or the repurposing of metformin (24) suggests therapeutic value for modulators of mTORC1 signaling in cystinosis. Given that dietary restriction of nutrients (e.g., low protein diet and/or reductions of essential and/or branched amino acids, including cystine) promote homeostasis by switching mTORC1 signaling off (38), combinations of nutritional interventions with existing and/or emerging drugs might have translatable potential in cystinosis and other currently intractable diseases.

In summary, our work describes a fundamental role of CTNS-cystine-mTORC1 signaling node as a guardian of cellular homeostasis and identifies an evolutionarily conserved lysosome-based signal that instructs fate specification in the epithelial cells of the kidney tubule. Modulating this pathway may yield therapeutic strategies for cystinosis and other lysosomal disorders, while creating opportunities to regulate homeostasis in specialized cell types.

METHODS

Antibodies and reagents

The following antibodies were used in this study: anti-LAMP1 (Santa Cruz Biotechnology, sc-19992, 1:1000); anti-LC3 (PM036, MBL, 1:200); anti-p62/SQSTM1 (PM045, MBL, 1:200); anti-phospho-S6 Ribosomal Protein (Ser235/236; Cell signaling technology, 4858, 1:500), anti-cathepsin D (Santa Cruz Biotechnology, sc-6486, 1:500), anti-S6 Ribosomal Protein (Cell Signaling Technology, 2217, 1:500), anti-phospho□4E-BP1 (Ser65; Cell signaling technology, 9451, 1:500), anti-4E-BP1 (Cell Signaling Technology, 9644, 1:500), anti-phospho-p70 S6 kinase 1 (Thr389; Cell Signaling Technology, 9234, 1:500); anti-p70 S6 kinase 1 (Cell Signaling Technology, 2708, 1:500), anti-acetyl□CoA carboxylase (Cell signaling, 3662, 1:500); anti-phospho□acetyl□CoA carboxylase (Ser79; Cell signaling, 3661, 1:500); anti-AMPKα (Cell signaling, 2793, 1:500); anti-phospho□AMPKα (Thr172; Cell signaling, 2535, 1:500), anti-TFE3 (Sigma, HPA023881, 1:500); anti-mTOR (Cell Signaling Technology, 7C10, 1:400 for immunofluorescence studies), anti-Raptor (2280, Cell Signaling Technology, 2280, 1:400); anti–RagC (Cell Signaling Technology, 5466, 1:500); rabbit anti-phospho-AKT (Ser473; Cell Signaling Technology, 13038, 1:500), anti-AQP1(Aviva Systems Biology, OASA00210, 1:400), anti-PCNA (Dako, M0879, 1:500), anti-α-tubulin (Sigma Aldrich, T5168; 1:1000), anti-Cyclin A2 (Abcam, Ab181591; 1:400), anti Cdc20 (Santa Cruz, sc-13162, 1:400), anti-Golgin-97 (Cell Signaling Technology, 13192; 1:400); anti-VDAC (Cell Signaling Technology; 4866, 1:400), anti-PMP70 (Sigma, SAB4200181, 1:500), anti-calreticulin (Cell Signaling Technology, 12238, 1:400), anti-β-actin (Sigma-Aldrich, A5441, 1:1000), anti-γ-tubulin (Sigma Aldrich, clone GTU-88,1:10000), and anti-HA (Roche, 11867423001; 1:500). Compounds included Bafilomycin A1 (Bfn A1; Enzo Life Sciences, ALX-380-030, 250 nM), ATP-competitive mTOR inhibitor Torin1 (TOCRIS Bioscience, CAS 1222998-36-8, 250 nM), Cysteamine (Sigma Aldrich, M6500-25G, 100µM), alcohol ester derivates of cystine (CDME, Sigma Aldrich 857327-5G, 0.05 mM), L-amino acid cystine (Sigma Aldrich, C7602–25G, 0.05 mM), and the biotinylated Lotus Tetragonolobus Lectin

(LTL; Vector Laboratories, B–1325). The cells used in this study were negatively tested for mycoplasma contamination using MycoAlert™ Mycoplasma Detection Kit (LT07-118, Lonza, Switzerland).

Generation and maintenance of ctns zebrafish

The *ctns*–specific left and right TALENs (*ctns*-TALENs) were constructed in according to Golden Gate TALEN assembly protocol and using the Golden Gate TALEN and TAL Effector Kit 2.0 (Addgene, Kit #1000000024). CIscript-GoldyTALEN was a gift from Daniel Carlson & Stephen Ekker (Addgene, plasmid # 38142). TALENs were designed with the TAL Effector Nucleotide Targeter 2.0 software on the Website of Cornell University. The TALENs target the exon 3 of *ctns* zebrafish gene: left TALEN-F: TCTTTTAATCCTTTGTGTTCACA and right TALEN-R: CATCTGTAACGGTTTATTTCAAT. The spacer between two TALEN target sites is ~15 nucleotides and contains an AciI restriction site in the middle, which is used for mutant screening. The TALEN expression plasmids were linearized with BamHI and then used for *in vitro* transcription (mMESSAGE mMACHINE T3 kit, Ambion). Approximately 1 nL of TALEN messenger ribonucleic acid (mRNAs, 400 ng/µL) was injected into one-cell stage zebrafish (*Danio rerio*) embryos. After 24 h, genomic DNA was extracted from injected embryos with normal appearance. Targeted genomic loci were amplified by using primers designed to anneal approximately 240 base pairs, and mutant allele was detected by AciI digestion of PCR product. The TALEN injected embryos were raised to adulthood (F0) and outcrossed with wild-type zebrafish. The embryos were then raised to adulthood (F1) for screening of heterozygous carriers. We identified a heterozygous carrier harboring *ctns* $^{+/del8}$ mutation and (F1) generations were crossed for obtaining homozygous mutant carrying *ctns*$^{del8/del8}$. Zebrafish were kept at day/night cycle of 14/10 h at 28°C. Stable zebrafish line expressing mCherry::1/2 vitamin D binding protein in the liver was established and outcrossed with *ctns*$^{+/del8}$ zebrafish to generate transgenic mutant line, which was crossed with *ctns*$^{+/del8}$ zebrafish to produce homozygous larvae, and the measurement of mCherry::1/2 vdbp was assessed by ELISA. Where indicated, zebrafish larvae were treated

at 5 dpf with system water containing DMSO or Rapamycin at different concentrations (50, 100 and 200 nM, Sigma Aldrich) for 9 days. The experimental protocols were approved by the appropriate licensing committee (Kanton Zürich Gesundheitsdirektion Veterinäramt; protocol ZH230/2018) at the University of Zurich.

Zebrafish urine collection and ELISA mCherry measurement

Zebrafish larvae were placed in a 96-well microplate with one larvae/100ml E3 medium/well and kept at 28C for 16 hours, followed by urine collection for ELISA assay (23). Liver and kidney tissues were extracted using 1x Cell Extraction Buffer PTR and diluted with Sample Diluent NS from the mCherry ELISA kit (Abcam, ab221829). 1/2vdbp-mCherry was assayed according to manufacturer's protocol, which is briefly as follows: 50 mL of E3 medium containing urine was distributed to a 96-well microplate pre-coated with anti-mCherry antibody. A 50 mL mixture of capture antibody and detector antibody was added to each well and incubated at 37°C for 1 hour. The wells were rinsed three times with 1 Wash Buffer PT and incubated with 100ml of TMB Substrate at room temperature for 10 minutes. The reaction was stopped by adding 100ml of stop solution, followed by reading the absorbance of each well at 450 nm.

Rodent models

Experiments were conducted on age– and gender–matched *Ctns* knockout mouse (C57BL/6 background) (4) or rat (Sprague–Dawley background) (18) lines, and their corresponding control littermates. Rats and mice were maintained under temperature-and humidity-controlled conditions with 12 h light/12 h dark cycle with free access to appropriate standard diet in accordance with the institutional guidelines of National Institutes of Health Guide for the Care and Use of Laboratory Animals. Kidneys were collected for analyses at the time of sacrifice. The experimental protocols were approved by the appropriate licensing committee (Kanton Zürich Gesundheitsdirektion Veterinäramt; protocol ZH230/2019, ZH195/2020) at the University of Zurich.

Rats aged 12 weeks were subcutaneously implanted with a slow-release pellet (Innovative Research of America, FL, USA). The pellets were designed to allow a constant release of Rapamycin (1.5mg/kg B.W./day, R-5000, LC Laboratories, Woburn, MA). Control animals received a placebo pellet equivalent to their respective rapamycin group. After 2 weeks of treatment, the rats were sacrificed, and kidney tissues were collected for analyses.

Kidney function

The mice were placed overnight in metabolic cages with ad libitum access to food and drinking water; urine was collected on ice, body weight, water intake and diuresis were measured. Blood (from sublingual vein) was obtained after anesthesia with ketamine/xylazine or isoflurane. Urea and creatinine were measured using UniCel DxC 800 pro Synchron (Beckman Coulter, Fullerton, CA, USA). Urinary levels of low-molecular weight Clara cell protein (CC16) were measured by using an enzyme-linked immunosorbent assay in according to the manufacturer's instructions (BIOMATIK EKU03200, Thermo Fischer Scientific, Waltham, MA).

Primary cultures of mouse proximal tubular cells

The kidneys were harvested from *Ctns* knockout mice and from their corresponding control littermates: one kidney was split transversally, and one half was fixed and processed for immunostaining while the other half was flash-frozen, homogenized by Dounce homogenizer in 1 mL of RIPA buffer that contains protease and phosphatase inhibitors and processed for western blot analysis. The contralateral kidney was taken to generate primary cultures of mPTCs (5,7). Freshly microdissected PT segments were seeded onto collagen-coated chamber slides (C7182, Sigma-Aldrich) and/or collagen coated 6- or 24-well plates (145380 or 142475, Thermo Fisher Scientific), and cultured at 37°C and 5% CO_2 in DMEM/F12 (21041-025, Thermo Fisher Scientific) with 0.5% dialyzed fetal bovine serum (FBS), 15mM HEPES (H0887, Sigma-Aldrich), 0.55mM sodium pyruvate (P2256, Sigma Aldrich), 0.1ml L^{-1} non-essential amino acids (M7145, Sigma Aldrich), hydrocortisone, human EGF, epinephrine, insulin, triiodothyronine, TF, and gentamicin/amphotericin (Single Quots® kit,

CC 4127, Lonza), pH 7.40, 325mOsm kg^{-1}. The medium was replaced every 48 h. Confluent monolayers of mPTCs were expanded from the tubular fragments after 6–7 days, characterized by a high endocytic uptake capacity. These cells were negatively tested for mycoplasma contamination.

Cystine measurements

Mouse or rat kidney tissue, or zebrafish embryos or primary cultured cells were homogenized and lysed with N-ethylmaleimide (NEM) solution containing 5.2 mmol l−1N-ethylmaleide in 10mmol L^{-1}potassium phosphate buffer adjusted to pH 7.4. The lysates were collected and precipitated with sulfosalicylic acid (12% w/v) and centrifuged at 10,000 rpm. for 10 min at 10 °C. The resulting supernatant was dissolved in citrate loading buffer (Biochrom Ltd, Cambridge, UK) and 50µl of this solution was analysed by Biochrom 30 Plus Amino Acid Analyzer (Biochrom Ltd). The protein pellet was dissolved in 0.1 mol L^{-1}NaOH solution and the protein concentration was determined by Biuret method. The concentration of amino acids was measured by using a lithium high performance physiological column followed by post-column derivatization with ninhydrin. The amino acids were identified according to the retention time and the ratio of the area between the two wavelengths (570nm and 440 nm) and quantified by using EZChrom Elite software (Agilent Technologies Inc., Pleasanton, California, USA). Cystine concentration was normalized to the protein concentration and reported in nmol per mg protein.

Nutrient starvation protocols and cell treatments

The withdrawal of serum, glucose, and amino acid was performed by washing mPTCs with Hank's balanced salt solution (55021 C, Sigma-Aldrich) and placing them in normal growth and nutrient–deprived medium (amino acid-free RPMI, starvation medium) for 4h. For amino acid starvation and stimulation experiments, the primary cells were rinsed twice with and incubated for 2h starvation medium or incubated in starvation medium and then stimulated with acid-free RPMI supplemented for 60 minutes with a standard amino acid mixture composed of MEM nonessential amino acid solution, MEM essential amino acid solution,

and L–glutamine (Invitrogen, Thermo Fisher Scientific) and with 0.5 % fetal calf serum that had been dialyzed against phosphate–buffered saline (PBS) in dialysis cassettes (Thermo Scientific) having an 3500 molecular weight cut–off. Where indicated, lysosomal proteolysis was inhibited by addition of BfnA1 (250 nM in cell culture medium for 4 h). Where indicated, the cells were treated with ATP–competitive mTORC1 inhibitor Torin1 (250nM in cell culture medium for 16h) or cysteamine (100 μM in cell culture medium for 16h). Where indicated, mPTCs were exposed to alcohol ester derivates of cystine (CDME, 0.1 mM) and L–amino acid cystine (0.1 mM) at the indicated time point. Afterwards, the cells were processed and analysed as described below.

Adenovirus transduction

For RNA interference studies, the adenovirus constructs include scrambled short hairpin (Scmb) or shRNAs targeting mouse *Raptor*. For expression studies, adenoviral constructs used include CMV (control vector, Ad-CMV-GFP, Vector Biolabs) or an individually carrying mouse hemagglutinin (HA) tagged-*Ctns or* carrying mouse HA tagged-mutant *Ctns* (Gly339Arg; $CTNS^{G339R}$) or 3×HA-tagged TMEM192 or expressing mouse green fluorescent protein (GFP)-tagged-*Map1lc3b* or expressing mouse red fluorescent protein (RFP)-tagged-*Lamp1*. The adenoviral constructs were purchased from Vector Biolabs (University City Science Center, Philadelphia, USA). The cells were plated onto collagen-coated chamber slides or 24-well or 6-well tissue culture plates. 24 h after plating the cells with approximately 70-80% confluence, adenovirus transduction was performed by incubating the cells for 16 h at 37°C with culture medium containing the virus. The cells were then challenged with fresh culture medium every 2 days, cultured for 2 days for the expression studies, 5 days for RNA interference studies, and collected for analyses.

Microarray and bioinformatics analysis

The Affymetrix (GeneChip mouse genome 430A 2.0 array) hybridization experiments were performed in triplicate at the Coriell Genotyping and Microarray Center (Coriell Institute for

Medical Research, Camden, New Jersey, USA) on total RNA extracted from microdissected proximal tubules of *Ctns* knockout mouse kidneys and controls. Normalized expression levels were generated from the raw intensities using the RMA method implemented in oligo Bioconductor package (39). Differentially expressed probes between conditions (*Ctns* knockout versus controls) were identified using the Bioconductor package limma (39). *P* values were corrected for multiple testing using the Benjamin–Hochberg method. The probes were annotated using the mouse430a2.db Bioconductor Annotation package. Pathway enrichment analysis was performed using the function enrichPathway from the Bioconductor package ReactomePA, run with the default parameters, selecting "mouse" as organism, and using all the genes on the microarray as universe. The analysis was performed separately for the up-regulated and the down-regulated genes. The modules associated with mouse cystinosin gene were determined using GeneBridge toolkit (www.systems-genetics.org).

Proteomics

Sample preparation: Cell pellets (~5×10^5 cells; n=3 mice per each group) were solubilized in 100µl of lysis buffer, treated with High Intensity Focused Ultrasound (HIFU) for 1 minute at an ultrasonic amplitude of 85%, and boiled at 95°C for 10 minutes. Proteins were extracted using a tissue homogenizer (Tissue Lyser II, QUIAGEN) for 2 cycles of 2 minutes at 30 Hz, boiled at 95°C for another 10 minutes, and subjected to a last cycle of 1 min of HIFU. The samples were centrifuged at 20000*g* for 10 min, and the protein concentration was determined using a Lunatic (Unchained Labs) instrument. For each sample, 50 µg of protein were taken. The samples were digested by adding 10µl of the 'Digest' solution. After 60 min of incubation at 37°C the digestion was stopped with 100µl of Stop solution. The solution was transferred to the cartridge and were removed by centrifugation at 3800 × g, while the peptides were retained by the iST-filter. Finally, the peptides were washed, eluted, dried and re-solubilized in 40µl of 3% acetonitrile, 0.1% FA. 1 µl of iRT peptides (Biognosys) at 1:100 dilution was added to each sample.

Liquid chromatography-mass spectrometry analysis: Mass spectrometry analysis was performed on an Orbitrap Fusion Lumos (Thermo Scientific) equipped with a Digital PicoView source (New Objective) and coupled to a M–Class UPLC (Waters). Solvent composition at the two channels was 0.1% formic acid for channel A and 0.1% formic acid, 99.9% acetonitrile for channel B. For each sample 1µl of peptides were loaded on a commercial MZ Symmetry C18 Trap Column (100Å, 5 µm, 180 µm × 20 mm, Waters) followed by nanoEase MZ C18 HSS T3 Column (100Å, 1.8 µm, 75 µm × 250 mm, Waters). The peptides were eluted at a flow rate of 300 nl/min by a gradient from 5 to 22% B in 80 min and 32% B in 10 min after an initial hold at 5% B for 3 min. The column was washed with 95% B for 10 min and afterwards the column was re-equilibrated to starting conditions for additional 10 min. Samples were acquired in a randomized order. The mass spectrometer was operated in data-dependent mode (DDA) acquiring a full-scan MS spectra (300−1’500 m/z) at a resolution of 120’000 at 200 m/z after accumulation to a target value of 500’000. Data-dependent MS/MS were recorded in the linear ion trap using quadrupole isolation with a window of 0.8 Da and HCD fragmentation with 35% fragmentation energy. The ion trap was operated in rapid scan mode with a target value of 10’000 and a maximum injection time of 50ms. Only precursors with intensity above 5’000 were selected for MS/MS and the maximum cycle time was set to 3 s. Charge state screening was enabled. Singly, unassigned, and charge states higher than seven were rejected. Precursor masses previously selected for MS/MS measurement were excluded from further selection for 20 s, and the exclusion window was set at 10 ppm. The samples were acquired using internal lock mass calibration on m/z 371.1012 and 445.1200. The mass spectrometry proteomics data were handled using the local laboratory information management system (LIMS).

Protein identification and label free protein quantification: The acquired raw MS data were processed by MaxQuant (version 1.6.2.3), followed by protein identification using the integrated Andromeda search engine. Spectra were searched against a Swissprot canonical mouse proteome (version from 2019-07-09), concatenated to its reversed decoyed fasta

database and common protein contaminants. Carbamidomethylation of cysteine was set as fixed modification, while methionine oxidation and N-terminal protein acetylation were set as variable. Enzyme specificity was set to trypsin/P allowing a minimal peptide length of 7 amino acids and a maximum of two missed cleavages. MaxQuant Orbitrap default search settings were used. The maximum false discovery rate (FDR) was set to 0.01 for peptides and 0.05 for proteins. Label free quantification was enabled and a 2 min window for match between runs was applied. In the MaxQuant experimental design template, each file is kept separate in the experimental design to obtain individual quantitative values. Protein fold changes were computed based on Intensity values reported in the proteinGroups.txt file. A set of functions implemented in the R package SRM Service was used to filter for proteins with 2 or more peptides allowing for a maximum of 3 missing values, and to normalize the data with a modified robust z-score transformation and to compute p-values using the *t*-test with pooled variance. If all measurements of a protein are missing in one of the conditions, a pseudo fold change was computed replacing the missing group average by the mean of 10% smallest protein intensities in that condition.

Metabolomics

Sample preparation: Cell pellets (~5×10^5 cells; n=3 mice per each group) were lysed and extracted with 500µL lysis solution (methanol: water 4:1, v/v) by vortexing for 30 min at 4°C. Precipitated proteins were pelleted by centrifugation (16,000*g*, for 15 min at 4 °C) and 50uL of the supernatants (50µL) were transferred to a clean Eppendorf vial. The transferred aliquot of the supernatants was kept at 35°C and dried down under a gentle flow of nitrogen. The dried extracts were reconstituted in 20uL water and 80uL injection buffer. 50uL of the reconstituted extract was transferred to a glass vial with narrowed bottom (Total Recovery Vials, Waters) for LC-MS injection. In addition, method blanks, QC standards, and pooled samples were prepared in the same way to serve as quality controls for the measurement. Injection buffer was composed of 90 parts of acetonitrile, 9 parts of methanol and 1 part of 5M ammonium acetate.

Liquid chromatography/mass spectrometry analysis: Metabolites were separated on a nanoAcquity UPLC (Waters) equipped with a BEH Amide capillary column (150 µm x50mm, 1.7µm particle size, Waters), applying a gradient of 5mM ammonium acetate in water (A) and 5mM ammonium acetate in acetonitrile (B) from 5% A to 50% A for 12min. The injection volume was 1µL. The flow rate was adjusted over the gradient from 3 to 2 µl/min. The UPLC was coupled to Synapt G2Si mass spectrometer (Waters) by a nanoESI source. MS1 (molecular ion) and MS2 (fragment) data was acquired using negative polarization and MS^E over a mass range of 50 to 1200 m/z at MS1 and MS2 resolution of >20'000.

Untargeted metabolomics data analysis: Metabolomics data sets were evaluated in an untargeted fashion with Progenesis QI software (Nonlinear Dynamics, Waters), which aligns the ion intensity maps based on a reference data set, followed by a peak picking on an aggregated ion intensity map. Detected ions were identified based on accurate mass, detected adduct patterns and isotope patterns by comparing with entries in the Human Metabolome Data Base (HMDB). A mass accuracy tolerance of 5mDa was set for the searches. Fragmentation patterns were considered for the identifications of metabolites. All biological samples were analysed at in triplicate and quality controls were run on pooled samples and reference compound mixtures to determine technical accuracy and stability. List of ranked proteins and metabolites had crossed each other, and the enrichment pathway analysis was performed using the OmicsNet 2.0 software.

Reverse transcription-quantitative PCR

Total RNA was extracted from mouse tissues using Aurum™ Total RNA Fatty and Fibrous Tissue Kit (Bio–Rad, Hercules, CA). DNAse I treatment was performed to eliminate genomic DNA contamination. Total RNA was extracted from cell cultures with RNAqueous® kit (Applied Biosystems, Life Technologies). One µg of RNA was used to perform the reverse transcriptase reaction with iScript ™ cDNA Synthesis Kit (Bio-Rad). Changes in mRNA levels of the target genes were determined by relative RT–qPCR with a CFX96™ Real Time PCR Detection System (Bio-Rad) using iQ ™ SYBR Green Supermix

(Bio-Rad). The analyses were performed in duplicate with 100nM of both sense and anti-sense primers in a final volume of 20 µL using iQ™ SYBR Green Supermix (Bio-Rad). Specific primers were designed using Primer3 (Supplementary Table 3). PCR conditions were 95°C for 3 min followed by 40 cycles of 15 sec at 95°C, 30 sec at 60°C. The PCR products were sequenced with the BigDye terminator kit (Perkin Elmer Applied Biosystems) using ABI3100 capillary sequencer (Perkin Elmer Applied Biosystems). The efficiency of each set of primers was determined by dilution curves (Supplementary Table 3). The program geNorm version 3.4 was applied to characterize the expression stability of the candidate reference genes in kidneys and six reference genes were selected to calculate the normalization factor. The relative changes in targeted genes over *Gapdh* mRNAs were calculated using the $2^{-\Delta\Delta Ct}$ formula.

Endocytosis assay in mouse kidneys and derived PT cells

Mouse kidneys. Receptor-mediated endocytosis was monitored in the proximal tubule of mouse kidneys PTs by measuring the uptake of β-lactoglobulin (L3908, Sigma). Briefly, β-lactoglobulin was tagged with Cy5 using TM2 Ab labelling kit (Amersham) following the manufacturer's instructions. Fifteen minutes after tail-vein injection of Cy5-β-lactoglobulin (1 mg/kg B.W) mice were anesthetized and their kidneys were harvested and processed by confocal microscopy.

Primary PT cells. The endocytic uptake was monitored in mPTCs cells following incubation for 60 min at 4 °C with 50µg × ml^{-1}bovine serum albumin (BSA)–Alexa–Fluor–647 (A34785, Thermo Fisher Scientific) in complete HEPES-buffered Dulbecco's modified Eagle's medium. The cells were given an acid wash and warmed to 37 °C in growth cell medium for 15 min before being fixed and processed for immunofluorescence analyses.

Lysosomal degradation

The detection of lysosomal activity was performed in live in kidney cells by using Bodipy-FL-PepstatinA (P12271, Thermo Fischer Scientific) or MagicRed –$(RR)_2$ substrate (MR–CtsB; 938, Immunochemistry Technologies) according to the manufacturer's

specifications. The cells were pulsed with 1µM Bodipy□FL□Pepstatin A or with 1µM MagicRed –$(RR)_2$ in Live Cell Imaging medium for 1h at 37°C, fixed and subsequently analyzed by confocal microscopy. The number of PepstatinA□or MagicRed positive structures per cell were quantified by using the open-source cell image analysis software CellProfiler™ as described below.

Immunofluorescence and confocal microscopy

Fresh mouse and rat kidneys were fixed by perfusion with 50-60 mL of 4% paraformaldehyde in PBS (158127, Sigma-Aldrich), dehydrated and embedded in paraffin at 58C. Paraffin blocks were sectioned into consecutive 5µm-thick slices with a Leica RM2255 rotary microtome (Thermo-Fisher Scientific) on Superfrost Plus glass slides (Thermo-Fisher Scientific). Before staining, slides were deparaffinized in Xylenes (534056, Sigma-Aldrich) and rehydrated. Antigen retrieval was accomplished by heating the slides at 95°C for 10 min in 10 mM sodium citrate buffer (pH 6.0). The slides were quenched with 50 mM NH_4Cl, blocked with 3% BSA in PBS Ca/Mg (D1283, Sigma-Aldrich) for 30 min and stained with primary antibodies diluted in blocking buffer overnight at 4°C. After two washes in 0.1% Tween 20 (v/v in PBS), the slides were incubated with the corresponding fluorophore-conjugated Alexa secondary antibodies (Invitrogen) diluted in blocking buffer at room temperature for 1h and counterstained with 1µg Biotinylated Lotus Tetragonolobus Lectin (LTL; B-1325 Vector Laboratories) and 1µM 4',6-Diamino-2-phenylindole dihydrochloride (DAPI; D1306, Thermo Fischer Scientific). The slides were mounted in Prolong Gold Anti□fade reagent (P36930, Thermo Fisher Scientific) and analyzed by confocal microscopy. The images were acquired using Leica SP8 confocal laser scanning microscope (Center for Microscopy and Image Analysis, University of Zurich) equipped with a Leica APO 63x NA 1.4 oil immersion objective at a definition of 1,024 x 1,024 pixels (average of eight or sixteen scans), adjusting the pinhole diameter to 1 Airy unit for each emission channel to have all the intensity values between 1 and 254 (linear range). The micrographs were processed with Adobe Photoshop (version CS5, Adobe System Inc., San Jose, USA) software. Quantitative

image analysis was performed by selecting randomly ~5-10 visual fields per each slide that included at least 3-5 PTs (LTL-positive or AQP1-positive where indicated), using the same setting parameters (pinhole, laser power, and offset gain and detector amplification below pixel saturation). For PCNA staining on rat kidney tissue following mTOR inhibition, the kidney sections were analyzed using a fluorescence microscope. The images were acquired using Leica Dmi8 wide-field fluorescence microscope equipped with a Leica HC PL APO x20/0.80 objective, and a Leica DFC9000 GTC camera. The full kidney slides were scanned and PCNA signal in the cortex of each kidney was quantified using the LASX software.
The cells were fixed for 10 min with 4% PFA in PBS, quenched with 50 mM NH_4Cl and permeabilized for 20 min in blocking buffer solution containing 0.1% Triton X-100 and 0.5% BSA dissolved in PBS. Subsequently, cells were incubated overnight with the appropriate primary antibodies at 4°C. After repeated washing with PBS, the slides were incubated for 45 min with the suitable fluorophore-conjugated Alexa secondary antibodies (Invitrogen), counterstained with 1µM DAPI for 5 min, mounted with the Prolong Gold Anti-fade reagent and analyzed by a Leica SP8 confocal laser scanning microscope (Center for Microscopy and Image Analysis, University of Zurich) using the settings described above. Quantitative image analysis was performed by selecting randomly 5 visual fields pooled from biological triplicates, with each field including at least 10-15 cells, using the same setting parameters (e.g., pinhole, laser power, and offset gain and detector amplification below pixel saturation). The quantitative cell image analyses of subcellular structures were determined by using the open□source cell image analysis software CellProfiler™ (40). In particular, the specific module “Measure□Object□Intensity□Distribution” was used to score the number of Map1Lc3b, or PepA or MR–positive structures. The pipeline “Cell/particle counting and scoring the percentage of stained objects” was used to score the fractions of Lamp1-positive structures that were also positive for Map1Lc3b. The “Cytoplasm-Nucleus Translocation Assay” was used to score the numbers of Ybx3 and Pcna–positive nuclei. For quantification of colocalization, non–overlapping images were acquired from each coverslip. Raw,

unprocessed images were imported into FIJI v.2.0.0-rc-69/1.52i and converted to 8-bit images, and images of individual channels were thresholded independently to eliminate background and non-specific staining noise and converted to binary masks. Co-localization between Lamp1 and mTOR or RagC and Lamp1 was determined using the ‘‘AND’’ function of the image calculator. The number of cells and/or fields of views used per each condition and the number of biologically independent experiments are indicated in the figure legends.

Immunoprecipitation

The cells (~2000000 cells; n=2 mice per each group) were lysed in a buffer containing 25mM Tris/HCl adjusted to pH 7.4, 150mM NaCl, 1% NP-40, and 1mM EDTA, 5% glycerol, protease, and phosphatase inhibitors for 10 min at 4 °C. Lysates were centrifuged at 12,000 r.p.m. for 10 min and the supernatants were incubated with 50 µl anti–-HA magnetic beads (Thermo Fisher scientific, 88836) with end-over-end rotation for 16h at 4°C. The protein-bound beads were washed four times with fractionation buffer and proteins immunoprecipitated were reduced by the addition of 40µl of Laemmli sample buffer, heated at 95 °C for 5 min, and resolved on 12% SDS polyacrylamide gel electrophoresis (PAGE) gel, and analyzed by western blotting.

Lysosome immunoprecipitation

Cells transiently expressing T192-3×HA were lysed, and intact lysosomes were immunoprecipitated using anti-HA-conjugated Dynabeads (Thermo Scientific, 88837). Briefly, the cells were seeded in a 6–well plate at a density appropriate for them to reach confluency after 24 h. The medium was removed, the cell monolayers were scraped into 10 ml KPBS (136 mM KCl and 10 mM KH2PO4, pH 7.25, containing protease (Roche, 1836153001) and phosphatase inhibitors (PhosSTOP Sigma, 04906845001) and collected by centrifugation at 1,500 r.p.m. for 5 min. The pelleted cells were resuspended in a total volume of 1 ml KPBS and ~4×10^6 cells were mechanically broken by spraying 8–10 times through a 23G needle attached to a 1ml syringe, and then spun down at 2,000 r.p.m for

10min at 4°C, yielding a post nuclear supernatant (PNS). The post-nuclear supernatant was harvested, quantified using Bradford assay (Thermo-Fisher, 23246). Equal quantities of proteins from each condition were incubated with 50 µl anti-HA magnetic beads with end-over-end rotation for 1h at 4°C. The lysosome-bound beads were washed four times with KPBS. For immunoblotting analysis, anti-HA immunoprecipitates were reduced by the addition of 40µl of Laemmli sample buffer, heated at 95 °C for 5 min, and resolved on 12% SDS polyacrylamide gel electrophoresis (PAGE) gel, and analyzed by western blotting.
For cystine measurements on purified lysosomes, 50 µL of 80% MeOH was added to the beads bound to organelles and incubated for 5 mins at room temperature. The free amino acids were further derivatized before MS analysis. For whole cell lysate samples, 30 µL of supernatant were taken and mixed with 3 µL of 5 N NaOH in borate buffer to ensure the pH was below pH 9. For LysoIP, the samples were dissolved in 40 µL borate buffer from Waters. A mixture of 30 µL samples (both WCL and LysoIP), 5 µL borate buffer, 5 µL MSK-CAA-A2 internal standard mixture (1:5 dilution) and 10 µL AQC solution was added, giving a total volume of 50 µL and mixed thoroughly immediately after addition. After 10 mins incubation at 55°C, samples were loaded onto a Waters UPLC H-Class Plus system with an Acquity UPLC Qardupole Solvent Manager and Sample Manager. Derivatized amino acids were detected on a Waters QDa single quadrupole mass detector in positive mode. The Qda was operated by one MS, followed by selected ion monitoring (SIR) for each individual amino acid with defined retention window, shown in table below. The column temperature was maintained at 55 °C. The injection volume was 1 µL. Gradient elution was performed using 0.1% formic acid in water as eluent A and 0.1% formic acid in acetonitrile as eluent B. The flow rate was kept constant at 0.5 mL/ min with the following gradient (expressed as solvent B): Initial conditions: 1.0% B, 0.0–1min: 1% B, 1–4 min: 13.0% B, 4–8.5 min: 15.0% B, 8.5 -9.5 min: 95.0% B, 9.5-11.5 min: 95% B, 12-15 min: 1% B. The data acquisition and data analysis were done by Masslynx 4.2 (Waters).

Immunoblotting

Proteins were extracted from mouse tissues or cultured cells, lysed using a buffer containing protease (Roche) and phosphatase inhibitors (PhosSTOP Sigma), followed by sonication and centrifugation at 16,000*g* for 10 min at 4°C. The samples were thawed on ice, normalized for protein (20μg/lane), dissolved in Laemmli sample buffer and separated by SDS-PAGE under reducing conditions. After blotting onto PVDF and blocking with 5% non-fat milk (1706404, Bio-Rad Laboratories), the membranes were incubated overnight at 4°C with primary antibody, washed, incubated with peroxidase-labeled secondary antibody, and visualized with enhanced chemiluminescence (WBKLS0050, Millipore, Life technologies). Signal intensity was assessed by measuring the relative density of each band normalized to β–-actin, GAPDH or α-tubulin with ImageJ software.

Cell viability assay

The viability of mPTCs after drug treatments were assessed via MTT assay (ab211091, Abcam) in accordance with the manufacturer's instructions. Briefly, the cells were washed three times with PBS and then incubated with 0.5 mg/ml of MTT diluted in cell media. After 4 h of incubation at 37°C and until appearance of intracellular purple formazan crystals, the remaining crystals were dissolved with dimethyl sulfoxide (276855, Sigma-Aldrich) or SDS, and the absorbance measured at 570nm.

Cell growth and proliferation

To measure proliferation and growth, the cells were seeded in 24□well plates at a density of 2.0 × 104 cells per well. The cells were cultured for 4 days, and cell medium was renewed daily. Where indicated, the cells were treated with Torin1 (24h at the indicated concentrations), then trypsinized every 24 h and quantified using the countess automated cell counter TC10 automated cell counter (BIO–RAD). The time–course experiments were repeated three times.

Statistics and reproducibility

The plotted data were presented as mean ± standard error of the mean (SEM). Statistical comparisons between experimental groups were determined by using one-way analysis of variance (ANOVA) followed by Tukey's or Sidak's multiple comparison test test, when appropriate. When only two groups were compared, two tailed unpaired or paired Student's *t* tests were used as appropriate. The normality criteria (calculated by D'Agostino and Pearson *omnibus* normally test) were met. Non-parametric data were analysed using a Kruskal-Wallis test with Dunn's multiple comparison correction. The levels of statistical significance are indicated by symbols, and the *P*-values are indicated in the figure legends along with the statistical tests. All experiments reported here were performed at least two to three times independently, unless otherwise indicated in the figure legends. The investigators were not blinded to allocation during the experiments and outcome assessment. Graph Pad Prism software v. 7.0a (GraphPad software) was used for generating all statistical analyses.

Data availability

Source data and/or reagents supporting the findings of this study are available from corresponding authors, O.D. and A.L., upon reasonable request.

REFERENCES

1. van der Wijst, J., Belge, H., Bindels, R. J. M. & Devuyst, O. Learning Physiology From Inherited Kidney Disorders. *Physiol. Rev*. **99,** 1575-1653 (2019).
2. Town, M. et al. A novel gene encoding an integral membrane protein is mutated in nephropathic cystinosis. *Nat. Genet.* **18,** 319–324 (1998).
3. Kanarek N., Petrova B. & Sabatini D. M., Dietary modifications for enhanced cancer therapy. *Nature* **579**, 507-517 (2020).
4. Festa, B.P., Chen, Z., Berquez, M. et al. Impaired autophagy bridges lysosomal storage disease and epithelial dysfunction in the kidney. *Nat. Commun.* **9,** 161 (2018).
5. Cherqui, S. & Courtoy, P. The renal Fanconi syndrome in cystinosis: pathogenic insights and therapeutic perspectives. *Nat. Rev. Nephrol,* **13,** 115–131 (2017).
6. Liu, G. Y. & Sabatini, D. M. mTOR at the nexus of nutrition, growth, ageing and disease. *Nat. Rev. Mol. Cell Biol.* **21**, 183-203 (2020).
7. Anandapadamanaban, M. et al. Architecture of human Rag GTPase heterodimers and their complex with mTORC1. *Science* **366**, 203-210 (2019).
8. Rogala, K. B. et al. Structural basis for the docking of mTORC1 on the lysosomal surface. *Science* 366, 468-475 (2019).
9. Ballabio, A. & Bonifacino, J. S. Lysosomes as dynamic regulators of cell and organismal homeostasis. *Nat. Rev. Mol. Cell Biol.* **21**, 101-118 (2020).
10. Grahammer, F. et al. mTOR Regulates Endocytosis and Nutrient Transport in Proximal Tubular Cells. *JASN* **28**, 230-241 (2017).
11. Fantus, D. et al. Roles of mTOR complexes in the kidney: implications for renal disease and transplantation. *Nat. Rev. Nephrol.* **12**, 587-609 (2016).
12. Andrzejewska, Z. et al. Cystinosin is a Component of the Vacuolar H^+-ATPase-Ragulator-Rag Complex Controlling Mammalian Target of Rapamycin Complex 1 Signaling. *JASN* **27**, 1678-1688 (2016).

13. Jouandin, P. et al. Lysosomal cystine mobilization shapes the response of TORC1 and tissue growth to fasting. *Science* **375**, 736 (2022).
14. Dhillon, P. et al. The Nuclear Receptor ESRRA Protects from Kidney Disease by Coupling Metabolism and Differentiation. *Cell Metab.* **33**, 379-394 (2021).
15. Christensen, E. I. & Birn, H. Megalin and cubilin: multifunctional endocytic receptors. *Nat. Rev. Mol. Cell Biol.* **3,** 256-266 (2002).
16. Mossmann, D. Park, S. & Hall, M. N. mTOR signalling and cellular metabolism are mutual determinants in cancer. *Nat. Rev. Cancer* **18**, 744-757 (2018).
17. Zoncu, R. et al. mTORC1 Senses Lysosomal Amino Acids Through an Inside-Out Mechanism That Requires the Vacuolar H^+-ATPase. *Science* 334, 678-683 (2011).
18. Krohn, P. et al. Multisystem involvement, defective lysosomes and impaired autophagy in a novel rat model of nephropathic cystinosis. *Hum. Mol. Genet.* ddac033 (2022).
19. Brodin-Sartorius, A. et al. Cysteamine therapy delays the progression of nephropathic cystinosis in late adolescents and adults. *Kidney International* **81**, P179-189 (2012)
20. Kalatzis, V. et al. Molecular pathogenesis of cystinosis: effect of *CTNS* mutations on the transport activity and subcellular localization of cystinosin*. Hum. Mol. Genet.* **13**, 1361-1371 (2004).
21. Manifava, M. et al. Dynamics of mTORC1 activation in response to amino acids. *eLife* **5**, https://doi.org/10.7554/eLife.19960 (2016).
22. Dancey, J. et al. mTOR signaling and drug development in cancer. *Nat. Rev. Clin. Oncol.* **7,** 209–219 (2010).
23. Chen, Z. et al. Transgenic zebrafish modeling low-molecular-weight proteinuria and lysosomal storage diseases. *Kidney International* **97,** 1150–1163 (2020).
24. Kulkarni, A. S. et al. Benefits of Metformin in Attenuating the Hallmarks of Aging. *Cell Metab.* **32**, 15-30 (2020).

25. Mizushima, N. & Levine, B. Autophagy in Human Diseases. *N. Engl. J. Med.* **383**, 1564-1576 (2020).

26. Castellano, B. M. et al. Lysosomal cholesterol activates mTORC1 via an SLC38A9-Niemann-Pick C1 signaling complex. *Science* **355**, 1306–1311 (2017)

27. Davis, O. B. et al. NPC1-mTORC1 Signaling Couples Cholesterol Sensing to Organelle Homeostasis and Is a Targetable Pathway in Niemann-Pick Type C. *Dev. Cell* **56**, 260-276 (2021).

28. Bartolomeo, R. et al. mTORC1 hyperactivation arrests bone growth in lysosomal storage disorders by suppressing autophagy. *JCI* **127,** 3717-3729 (2017).

29. Ivanova, E. A., van den Heuvel, L. P. & Elmonem, M.A. et al. Altered mTOR signalling in nephropathic cystinosis. *J. Inherit. Metab. Dis.* **39,** 457–464 (2016).

30. Hollywood, J. A. et al. Use of human induced pluripotent stem cells and kidney organoids to develop a cysteamine/mTOR Inhibition combination therapy for Cystinosis. *JASN* **31**, 962-982 (2020).

31. Yu, Y. et al. Effects of simian virus 40 large and small tumor antigens on mammalian target of rapamycin signaling: small tumor antigen mediates hypophosphorylation of eIF4E-binding protein 1 late in infection. *J. Virol*. **79**, 6882-6889 (2005).

32. Gasnier, B. Plug-and-socket mechanisms in nutrient sensing by lysosomal amino acid transporters. *PNAS*, e2102173118 (2021).

33. Taylor, P. M. Amino acid transporters: eminences grises of nutrient signalling mechanisms? Biochem. Soc. Trans. 37, 237–241 (2009).

34. Rebsamen, M. et al. SLC38A9 is a component of the lysosomal amino acid sensing machinery that controls mTORC1. *Nature* **519,** 477-481 (2015).

35. Lei, H. et al. A conformational change in the N terminus of SLC38A9 signals mTORC1 activation. *Structure* **29**, 426-432 (2021).

36. Fromm, S. A., Lawrence, R. E. & Hurley J. H. Structural mechanism for amino acid-dependent Rag GTPase nucleotide state switching by SLC38A9. *Nat. Struct. Mol. Biol.* **27**, 1017-1023 (2020).

37. Schreiber, K. H., Arriola Apelo, S. I. & Yu, D. *et al.* A novel rapamycin analog is highly selective for mTORC1 in vivo. *Nat. Commun.* **10,** 3194 (2019).

38. Green, C. L., Lamming, D. W. & Fontana, L. Molecular mechanisms of dietary restriction promoting health and longevity. *Nat. Rev. Mol. Cell Biol.* **23**, 56-71 (2022).

39. Carvalho, B. S. & Irizarry, R. A. A framework for oligonucleotide microarray preprocessing. *Bioinformatics* **26**, 2363–2367 (2010).

40. Carpenter, A. E., Jones, T. R. & Lamprecht, M. R. et al. CellProfiler: image analysis software for identifying and quantifying cell phenotypes. *Genome Biol.* **7,** R100 (2006).

ACKNOWLEDGEMENTS

We thank Nadine Nägele for technical assistance, and Alessio Cremonesi and Benjamin Klormann for cystine measurements, and the Center for Microscopy and Image Analysis at the University of Zurich for providing equipment and confocal microscopy assistance as well as the Functional Genomics Center at the University of Zurich for providing equipment and assistance with sample preparation and mass spectrometry-based analyses. We also thank Chia-Wei Li and Paolo Nanni for their advice and fruitful discussions.

We acknowledge Euro-BioImaging (www.eurobioimaging.eu) for providing access to imaging technologies and services via the Italian Node (ALEMBIC, Milan, Italy). We are grateful to the Cystinosis Research Foundation (Irvine, CA, USA), the Swiss National Science Foundation (project grant 310030_189044), and the University Research Priority Program of the University of Zurich (URPP) ITINERARE - Innovative Therapies in Rare Diseases (OD and AL).

AUTHOR CONTRIBUTIONS

A.L. and O.D. conceptualized the overall study and supervised the work. A.L., M.B. and O.D. planned the overall experimental design. B.P.F. and M.B. performed cellular and mouse studies and analyzed and interpreted the data. Z.C. generated the *ctns* knockout zebrafish model and transgenic zebrafish line expressing a bona fide biosensor for PT function/LMW proteinuria, and together with S.K. performed zebrafish experiments, and analyzed the data. P.K. performed rat experiments and analyzed the data. S.P. and E.D. contributed to the analysis and interpretation of microarray data. M.B. performed lysosome purification, RNA interference, gene expression experiments, and molecular biology studies and analyzed the data. E.L. performed integrative metabolomics and contributed to analyze multi-omics data. A.L. and O.D. wrote the paper with inputs and comments from all the authors.

Competing interests: The authors declare no competing interests.

Figure Legends

Figure 1. Cystine storage and defective lysosome catabolism divert differentiation towards proliferation. (**a**) Cystine levels in *Ctns* mouse kidneys; n=6 animals per group. (**b**) Immunofluorescence and quantification of the Lamp1 mean fluorescence intensity (MFI) in LTL^+ PTs of *Ctns* kidneys, n>137 PTs pooled from three mice. (**c**) Immunofluorescence and quantification of the Cy5-tagged β-lactoglobulin MFI in LTL^+ PTs of *Ctns* kidneys, n>330 PTs pooled from three mice. (**d**) CC16 levels in urine samples from *Ctns* mice; n=7 biologically independent samples per each group. (**e**) Volcano plot of genome-wide changes in PT segments from *Ctns* kidneys. Red and green dots indicate the differentially expressed genes (DEGs; adjusted *p* value < 0.05; n=3 animals per group). (**f**) GSEA of enriched biological pathways of in $Ctns^{KO}$ associated DEGs. (**g**) Immunoblots and quantification of the indicated proteins in *Ctns* kidneys; n=3 animals per group. (**h**) Kidney tissues stained for Ccna2 (red), Megalin (blue), and PT marker (LTL, green). (**i**) Confocal microscopy and quantification of $BrdU^+$ cells (expressed as percentage of total cells; n>55 randomly selected fields of views per each condition). (**j**) Confocal microscopy and quantification of BSA^+ structures per cell (n>175 cells per each condition). (**k**) Quantification of GFP/RFP^+ structures in *Ctns* cells transiently expressing GFP:: Map1lc3b and Lamp1::RFP (expressed as percentage of total lysosomes; n=10 randomly selected fields of views per each condition). (**l**) Immunoblots and quantification of the indicated proteins in input samples and corresponding Lyso-IP fractions from *Ctns* mPTCs. n=3 biologically independent experiments. Plots represent mean ± SEM. Statistics calculated by unpaired two-tailed Student's *t* test. Dotted white squares contain images at high magnification. Nuclei counterstained with DAPI (grey). Scale bars are 50μm in **b**, **c**, and **h**, and 10μm in **j**, **k**, and **l**.

Figure 2. Hyperactive mTORC1 drives metabolic switch in CTNS-deleted/cystine accumulating PT cells. (**a**) Diagram of the multi-omics integration. (**b**-**c**) Volcano plot of (**b**) proteome and (**c**) metabolome changes induced by CTNS loss. Black dots indicate the

proteins and metabolites [Log_2 (fold change) < –0.5 and Log_2 (fold change) >1; and p–value < 0.05]. (**d,** left) Kyoto Encyclopaedia of Genes and Genomes pathway analysis; n=3 biologically independent samples. Black dashed line indicates the threshold of significant enrichment. Black circles indicate the size of enriched proteins/metabolites. (**d,** right) Diagram of upstream regulators of mTORC1 and its downstream regulated pathways. (**e**) Quantification of the indicated proteins; n=3 biologically independent replicates. (**f,** left) Diagram of the components forming V-ATPase-Ragulator-Rag lysosomal scaffold. (**f,** right) Immunoblots of the indicated proteins in input samples and corresponding Lyso-IP fractions from *Ctns*^{WT} and *Ctns*^{KO} mPTCs; n= 3 biologically independent experiments. (**g**) Immunofluorescence and quantification of RagC/Lamp1^{+} structures (expressed as percentage of total lysosomes; n=15 randomly selected fields of views per each condition). Dotted white squares contain images at high magnification. (**h**) Immunofluorescence and quantification of $^{pS235/236}$S6 MFI in Aqp1^{+} PTs (green) of rat *Ctns* kidneys; n>227 PTs pooled from 3 animals per each group. (**i**-**j**) Immunoblots and quantification of the indicated proteins in (**i**) 24-week-old *Ctns* rats or (**j**) 5-dpf-*ctns* zebrafish; n= 10 rats per group and n=7 biologically independent experiments (with each experiment representing a pool of 7 zebrafish). Plots represent mean ± SEM. Statistics calculated by unpaired two-tailed Student's *t* test. Nuclei counterstained with DAPI (grey). Scale bars are 10 μm in **g** and 50μm in **h**.

Figure 3. Temporal mTORC1 activation by cystine buildup leads to kidney disease development in CTNS deficient mice. (**a**) Quantification of LMW-Clara cell 16 (CC16) protein in the urine of *Ctns* mice at the indicated times (n>6 animals per each group/time point). (**b**) Cystine levels in *Ctns* kidneys (n>4 mice per each group). (**c**) Workflow for monitoring mTORC1 activity in *Ctns* mice. mPTCs from (**d** and **f**) asymptomatic (6 weeks old), (**e** and **g**) pre–symptomatic (12 weeks old), and (**i**) symptomatic (24 weeks old) *Ctns*^{KO} mice and their (age–matched) control littermates were cultured under fed and starved

conditions. (**d** and **e**) Immunoblots and quantification of the indicated proteins; n=3 mice per each group. (**f** and **g**) Immunofluorescence and quantification of $mTOR^{+}$-$Lamp1^{+}$ signals (n= 10 randomly selected and non-overlapping fields of views per each condition). Nuclei counterstained with DAPI (blue). (**h**) Fed mPTCs were treated with cysteamine (100 nM) or Torin1 (250 nM) for 16h. (**i**) Immunoblots of the indicated proteins; n=2 biologically independent experiments. (**j**) Cystine levels in *Ctns* mPTCs (n=6 biologically independent samples per each condition). Plots represent mean ± SEM. Statistics calculated by unpaired two-tailed Student's *t* test. Scale bars, 10μm.

Figure 4. Lysosomal cystine regulates mTORC1 activity through Ragulator-Rag GTPase lysosomal scaffold. (**a**-**d**) mPTCs from *Ctns*^{KO} mice were transduced with (**a**) Null or hemagglutinin–tagged $CTNS^{WT}$ ($CTNS^{WT}$–HA) or HA–tagged mutant CTNS ($CTNS^{G339R}$–HA) bearing adenoviral particles for 2 days. (**b**) Cystine levels in mPTCs; n=6 biologically independent experiments. (**c** and **h**) Cells were cultured under fed or starved conditions or restimulated by adding back amino acids and glucose (AA/G stim). (**c**) Immunoblots of the indicated proteins. (**d**) Fed *Ctns*^{KO} mPTCs transiently expressing tagged $CTNS^{WT}$ or $CTNS^{G339R}$ were lysed, and the samples were subjected to HA immunoprecipitation and immunoblotting for the indicated proteins. (**e**-**i**) Starved *Ctns*^{WT} mPTCs were exposed to (**e**) CDME (0.1 mM) or with unmodified L-cystine (0.1 mM) for the indicated times. (**f**) Cystine levels in *Ctns* mPTCs (n>4 biologically independent samples per each condition). (**g**) Cystine levels in whole cell lysates and purified lysosomes. n=2 biologically independent experiments. (**h**) Immunoblots of the indicated proteins; n=3 biologically independent experiments. Quantification of the indicated proteins are shown in Supplementary Fig.6g. (**i**) The cells were lysed, and the samples were subjected to HA immunoprecipitation and immunoblotting for the indicated proteins. n=2 biologically independent experiments in **c**, **d** and **i**. Plots represent mean ± SEM. Statistics calculated by Kruskal-Wallis followed by Dunn's multiple comparison test.

Figure 5. Suppressing mTORC1 rescues lysosome proteolysis and cell differentiation downstream of CTNS loss and cystine storage. (**a**-**j**) Cells were treated with vehicle (DMSO) or Torin1 (250nM for 16h). (**a**-**b**) Immunoblots and quantification of the indicated proteins. n= 3 (**a**) and 4 (**b**) biologically independent experiments. (**c**) Confocal microscopy and quantification of PepA$^+$ puncta per cell (n>247 cells per each condition pooled from three biologically independent experiments). (**d**) Oxygen consumption rates (OCRs) were measured under basal level and after the sequential addition of oligomycin (Oligo, 1 μM), FCCP (0.5 μM), and Rotenone (ROT; 1μM) + Antimycin A (ANT; 1μM); n = 3 biologically independent experiments. (**e**) Confocal microscopy and quantification of MitoSOX fluorescence intensity per cell (n>42 cells per each condition). Representative images are shown in Supplementary Fig. 7d. (**f**) Quantification of the number Ybx3$^+$ nuclei. (**g**) mRNA levels for the indicated genes; n>6 replicates pooled from 3 biologically independent experiments. (**h**) Quantification of the number of Pcna$^+$ nuclei; n=10 non-overlapping fields of views per each condition. (**i**) Growth curves in *Ctns* mPTCs; n=3 biologically independent experiments. (**j**) Confocal microscopy and quantification of BSA$^+$ structures per cell (n>175 cells per each condition). Plots represent mean ± SEM. Statistics calculated by one-way ANOVA followed by Tukey's or Sidak's multiple comparisons test in **b**, **c**, **g,** and **j**; and by unpaired two–tailed Student's *t* test in **d, e**, **f, h,** and **i**. Nuclei counterstained with DAPI (blue or grey). Scale bars, 10μm.

Figure 6. mTORC1 inhibition rescues PT dysfunction in a zebrafish model of cystinosis. (**a**) Diagram showing the generation of transgenic zebrafish line expressing a bona fide biosensor for LMW proteinuria. Fate of ½vdbp-mCherry under physiological conditions: ½vdbp-mCherry (~50 kDa) is (1) produced in liver, (2) secreted into the bloodstream and filtered by the glomerulus, (3) reabsorbed via receptor-mediated endocytosis by proximal tubule (PT) cells, and (4) processed by lysosomes. EE, early endosome; LE, late endosome; Lys, lysosome. (**b**-**e**) 5dpf-*ctns* zebrafish larvae stably expressing lfabp::1/2vdbp□mCherry were treated with vehicle or Rapamycin (200 nM) or

metformin (100 μM). (**b**-**d**) Immunoblotting and quantification of the indicated proteins, with each lane representing a pool of 6 zebrafish; n=4 biologically independent experiments in **b** and n=7 biologically independent experiments in **d**. (**c-e**) After 9 days of treatment, zebrafish and urine samples were harvested and analysed. Quantification of mCherry levels by ELISA; n= 11 vehicle-treated *ctns*^{WT} zebrafish; n=26 vehicle-treated *ctns*^{KO} zebrafish; and n=39 Rapa-treated *ctns*^{KO} zebrafish in **c** and n=23 vehicle-treated *ctns*^{KO} zebrafish; and n=23 metformin-treated *ctns*^{KO} zebrafish in **e**. Plots represent mean ± SEM. Statistics calculated by one-way ANOVA followed by Krusk-Wallis test in **d-e**. Scale bars, 50μm.

Figure 1

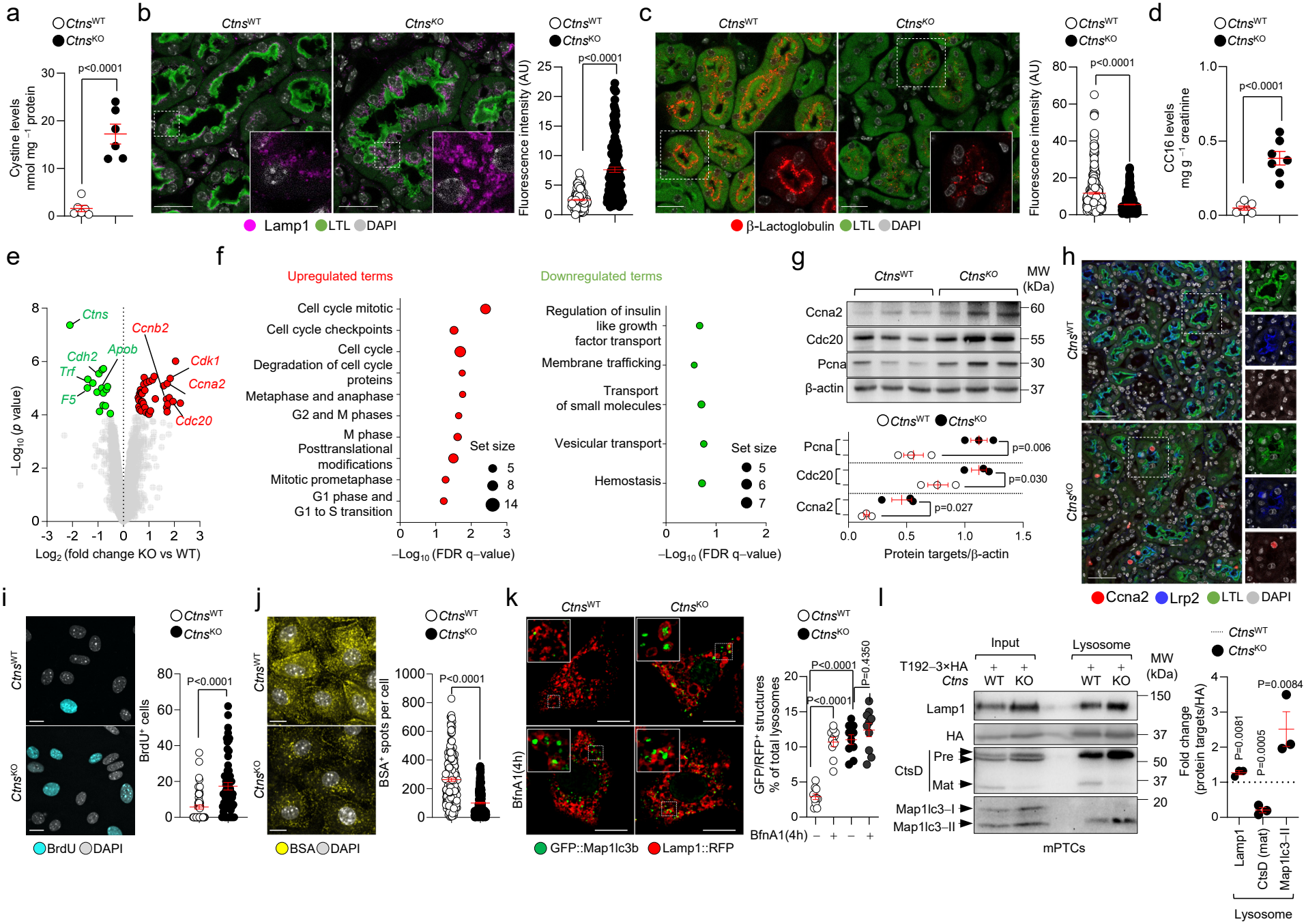
a
Ctns^WT
Ctns^KO
Cystine levels nmol mg −1 protein
p<0.0001
b
Ctns^WT
Ctns^KO
Lamp1 LTL DAPI
Fluorescence intensity (AU)
p<0.0001
c
Ctns^WT
Ctns^KO
β-Lactoglobulin LTL DAPI
Fluorescence intensity (AU)
p<0.0001
d
Ctns^WT
Ctns^KO
CC16 levels mg g −1 creatinine
p<0.0001
e
Ctns
Ccnb2
Apob
Cdh2
Trf
F5
Cdk1
Ccna2
Cdc20
−Log10 (p value)
Log2 (fold change KO vs WT)
f
Upregulated terms
Cell cycle mitotic
Cell cycle checkpoints
Cell cycle
Degradation of cell cycle proteins
Metaphase and anaphase
G2 and M phases
M phase
Posttranslational modifications
Mitotic prometaphase
G1 phase and G1 to S transition
Set size
5
8
14
−Log10 (FDR q−value)
Downregulated terms
Regulation of insulin like growth factor transport
Membrane trafficking
Transport of small molecules
Vesicular transport
Hemostasis
Set size
5
6
7
−Log10 (FDR q−value)
g
Ctns^WT
Ctns^KO
MW (kDa)
Ccna2
Cdc20
Pcna
β-actin
60
55
30
37
Ctns^WT Ctns^KO
Pcna
Cdc20
Ccna2
p=0.006
p=0.030
p=0.027
Protein targets/β-actin
h
Ctns^WT
Ctns^KO
Ccna2 Lrp2 LTL DAPI
i
Ctns^WT
Ctns^KO
BrdU DAPI
BrdU+ cells
P<0.0001
j
Ctns^WT
Ctns^KO
BSA DAPI
BSA+ spots per cell
P<0.0001
k
Ctns^WT
Ctns^KO
BfnA1(4h)
GFP::Map1lc3b Lamp1::RFP
GFP/RFP+ structures % of total lysosomes
P<0.0001
P<0.0001
P=0.4350
BfnA1(4h) − + − +
l
Input
Lysosome
T192−3×HA Ctns
WT KO WT KO
MW (kDa)
Lamp1
HA
CtsD
Pre
Mat
Map1lc3−I
Map1lc3−II
150
37
50
37
20
mPTCs
Ctns^WT
Ctns^KO
Fold change (protein targets/HA)
P=0.0081
P=0.0005
P=0.0084
Lamp1
CtsD (mat)
Map1lc3−II
Lysosome

Figure 2

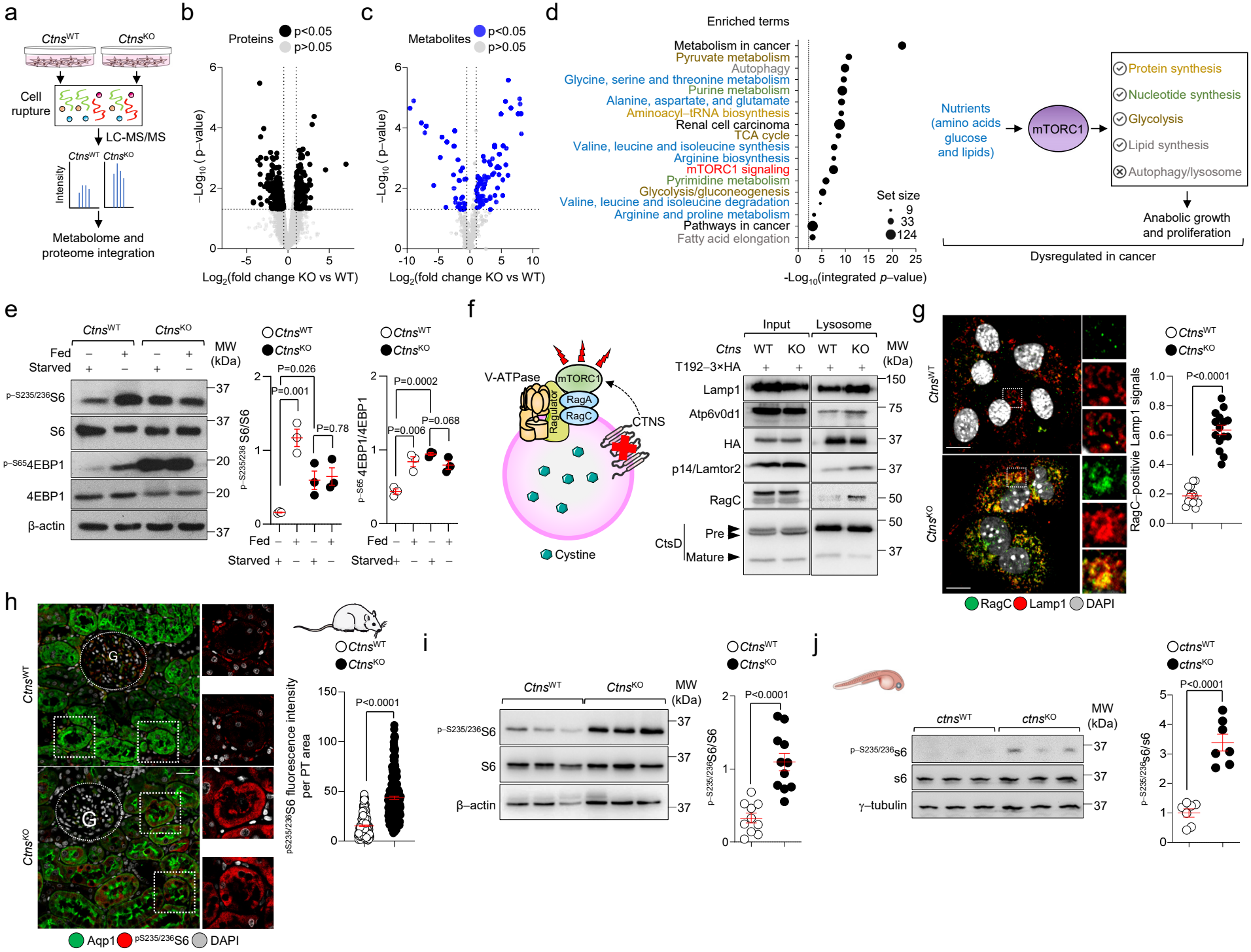
a
Ctns^WT
Ctns^KO
Cell rupture
LC-MS/MS
Intensity
Metabolome and proteome integration
b
Proteins
p<0.05
p>0.05
−Log10 (p−value)
Log2(fold change KO vs WT)
c
Metabolites
p<0.05
p>0.05
−Log10 (p−value)
Log2(fold change KO vs WT)
d
Enriched terms
Metabolism in cancer
Pyruvate metabolism
Autophagy
Glycine, serine and threonine metabolism
Purine metabolism
Alanine, aspartate, and glutamate
Aminoacyl−tRNA biosynthesis
Renal cell carcinoma
TCA cycle
Valine, leucine and isoleucine synthesis
Arginine biosynthesis
mTORC1 signaling
Pyrimidine metabolism
Glycolysis/gluconeogenesis
Valine, leucine and isoleucine degradation
Arginine and proline metabolism
Pathways in cancer
Fatty acid elongation
Set size
9
33
124
-Log10(integrated p−value)
Nutrients (amino acids glucose and lipids)
mTORC1
Protein synthesis
Nucleotide synthesis
Glycolysis
Lipid synthesis
Autophagy/lysosome
Anabolic growth and proliferation
Dysregulated in cancer
e
Ctns^WT
Ctns^KO
Fed
Starved
MW (kDa)
p−S235/236S6
S6
p−S65 4EBP1
4EBP1
β-actin
p−S235/236 S6/S6
P=0.026
P=0.001
P=0.78
p−S65 4EBP1/4EBP1
P=0.0002
P=0.006
P=0.068
f
V-ATPase
mTORC1
Ragulator
RagA
RagC
CTNS
Cystine
Input
Lysosome
Ctns
WT
KO
T192−3×HA
MW (kDa)
Lamp1
Atp6v0d1
HA
p14/Lamtor2
RagC
CtsD
Pre
Mature
g
Ctns^WT
Ctns^KO
RagC−positivie Lamp1 signals
P<0.0001
RagC
Lamp1
DAPI
h
Ctns^WT
Ctns^KO
Aqp1
pS235/236S6
DAPI
pS235/236S6 fluorescence intensity per PT area
P<0.0001
i
Ctns^WT
Ctns^KO
MW (kDa)
p−S235/236S6
S6
β−actin
p−S235/236S6/S6
P<0.0001
j
ctns^WT
ctns^KO
MW (kDa)
p−S235/236s6
s6
γ−tubulin
p−S235/236s6/s6
P<0.0001

Figure 3

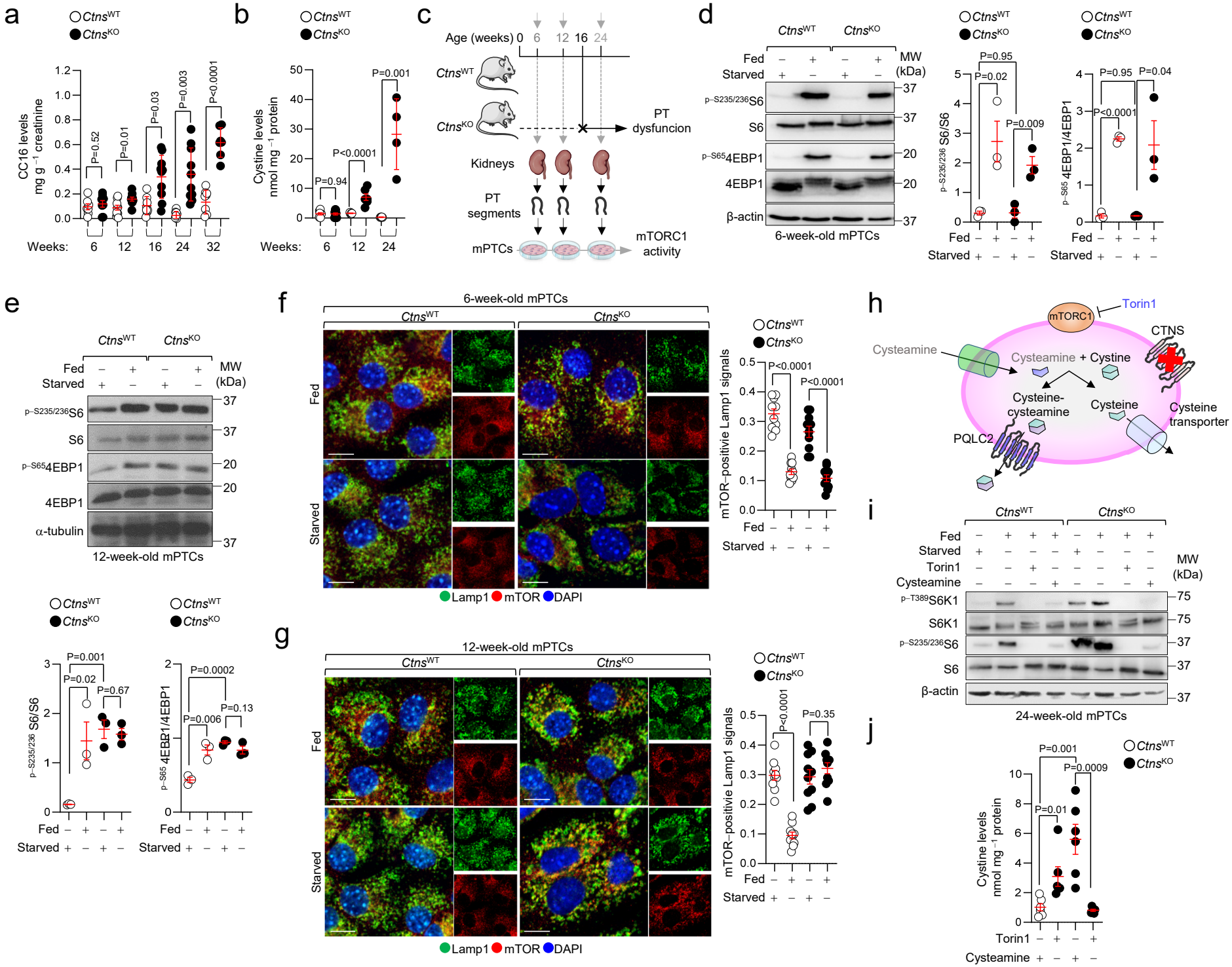
a
Ctns^WT
Ctns^KO
CC16 levels mg g⁻¹ creatinine
P=0.52
P=0.01
P=0.03
P=0.003
P<0.0001
Weeks: 6 12 16 24 32
b
Cystine levels nmol mg⁻¹ protein
P=0.94
P<0.0001
P=0.001
Weeks: 6 12 24
c
Age (weeks) 0 6 12 16 24
PT dysfuncion
Kidneys
PT segments
mPTCs
mTORC1 activity
d
Fed
Starved
MW (kDa)
p-S235/236S6
S6
p-S65 4EBP1
4EBP1
β-actin
6-week-old mPTCs
p-S235/236 S6/S6
p-S65 4EBP1/4EBP1
P=0.95
P=0.02
P=0.009
P=0.04
P<0.0001
e
α-tubulin
12-week-old mPTCs
P=0.001
P=0.02
P=0.67
P=0.0002
P=0.006
P=0.13
f
6-week-old mPTCs
Lamp1 mTOR DAPI
mTOR-positivie Lamp1 signals
P<0.0001
g
12-week-old mPTCs
P=0.35
h
Torin1
mTORC1
CTNS
Cysteamine
Cysteamine + Cystine
Cysteine-cysteamine
Cysteine
Cysteine transporter
PQLC2
i
Torin1
Cysteamine
p-T389S6K1
S6K1
24-week-old mPTCs
j
Cystine levels nmol mg⁻¹ protein

Figure 4

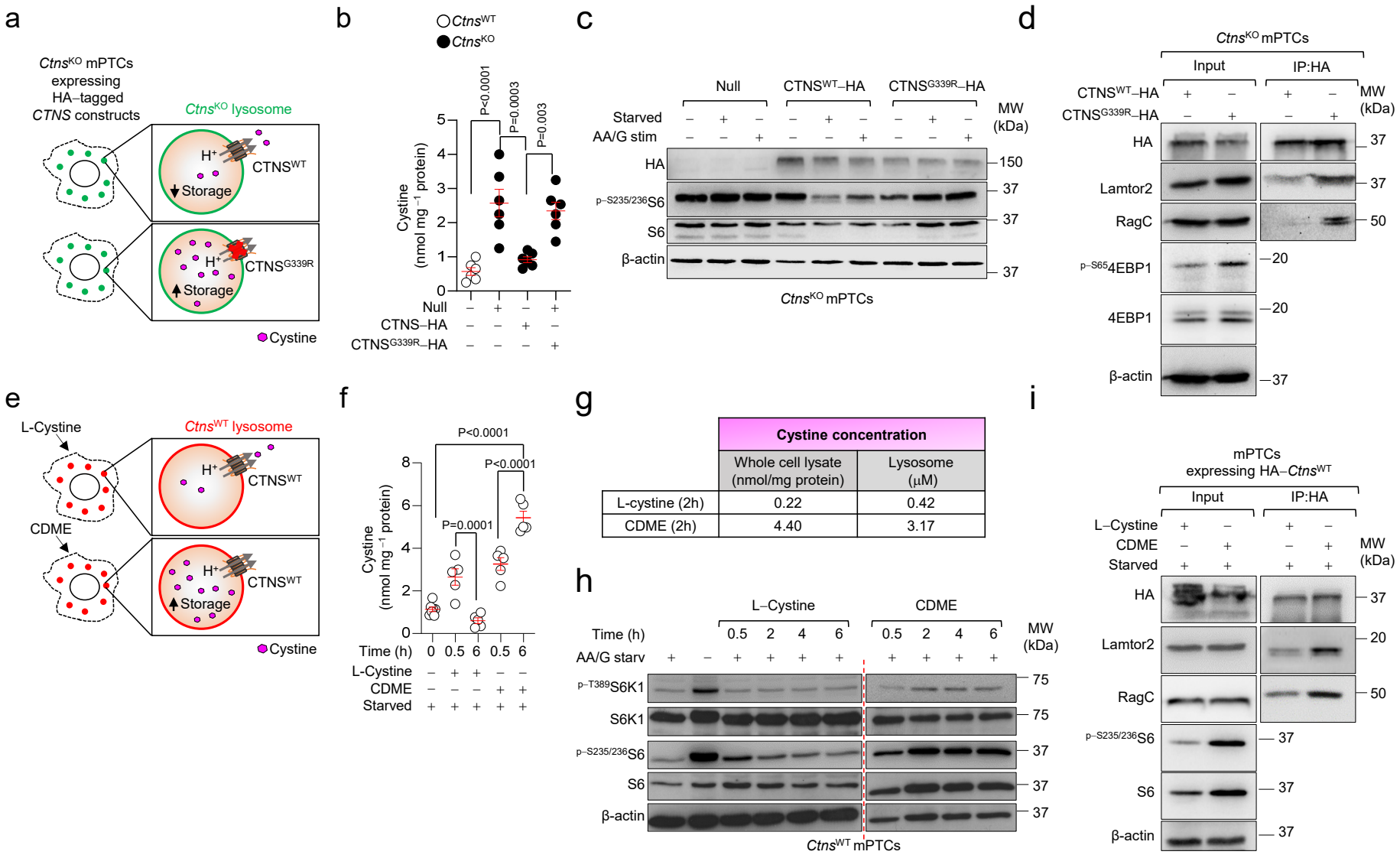
a
Ctns^KO mPTCs expressing HA–tagged CTNS constructs
Ctns^KO lysosome
H+
CTNS^WT
Storage
CTNS^G339R
Cystine
b
Ctns^WT
Ctns^KO
P<0.0001
P=0.0003
P=0.003
Cystine (nmol mg−1 protein)
Null
CTNS–HA
CTNS^G339R–HA
c
Null
CTNS^WT–HA
CTNS^G339R–HA
Starved
AA/G stim
MW (kDa)
HA
p–S235/236S6
S6
β-actin
150
37
Ctns^KO mPTCs
d
Ctns^KO mPTCs
Input
IP:HA
CTNS^WT–HA
CTNS^G339R–HA
HA
Lamtor2
RagC
p–S65 4EBP1
4EBP1
β-actin
20
50
e
L-Cystine
CDME
Ctns^WT lysosome
f
P<0.0001
P=0.0001
Time (h)
L-Cystine
CDME
Starved
g
Cystine concentration
Whole cell lysate (nmol/mg protein)
Lysosome (μM)
L-cystine (2h) 0.22 0.42
CDME (2h) 4.40 3.17
h
L–Cystine
CDME
Time (h)
AA/G starv
p–T389S6K1
S6K1
p–S235/236S6
S6
β-actin
75
Ctns^WT mPTCs
i
mPTCs expressing HA–Ctns^WT
Input
IP:HA
L–Cystine
CDME
Starved
HA
Lamtor2
RagC
p–S235/236S6
S6
β-actin
20
50

Figure 5

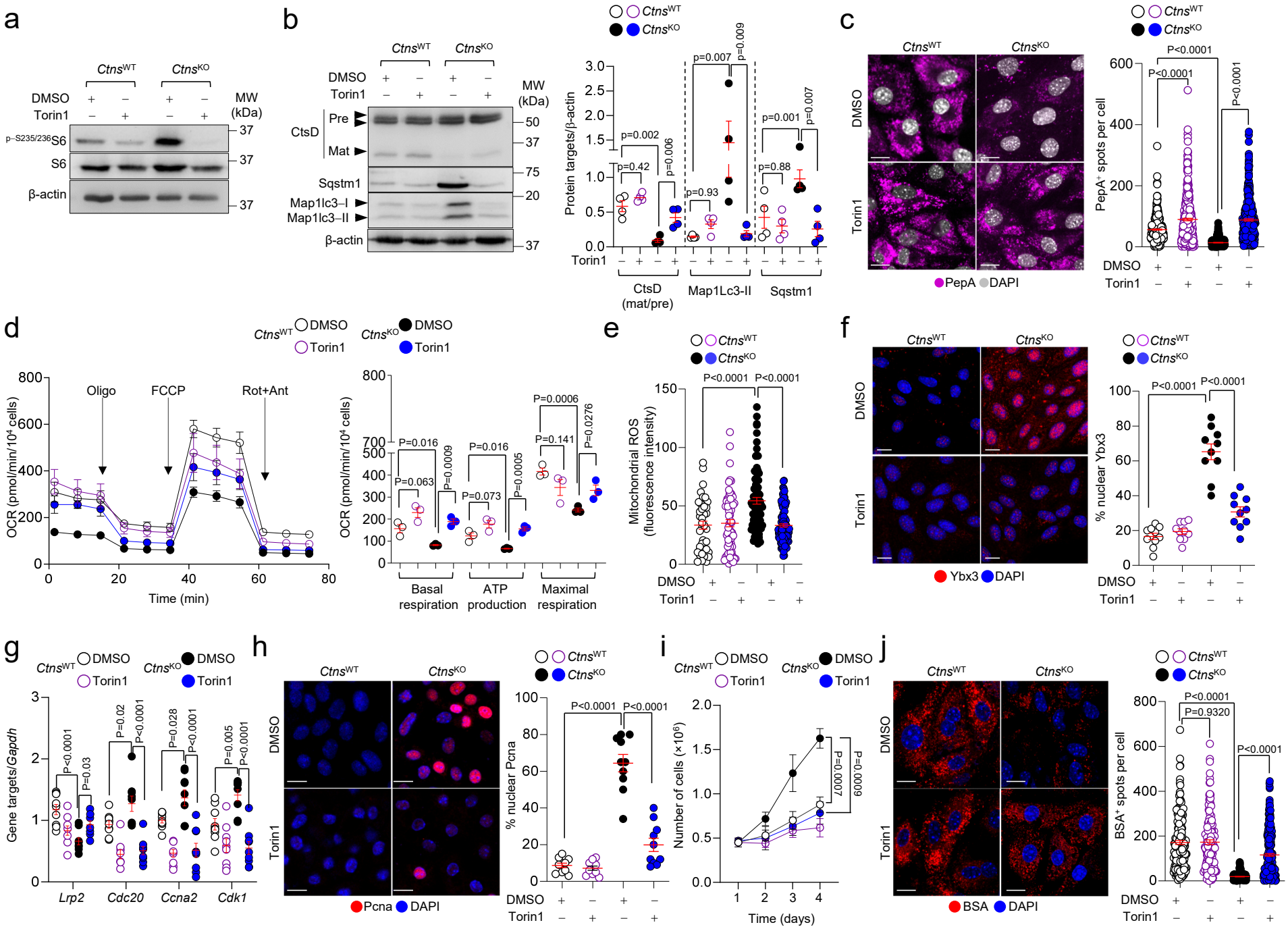
a
Ctns^WT
Ctns^KO
DMSO
Torin1
MW (kDa)
p-S235/236 S6
S6
β-actin
37
b
CtsD
Pre
Mat
Sqstm1
Map1lc3–I
Map1lc3–II
50
75
20
Protein targets/β-actin
p=0.002
p=0.42
p=0.006
p=0.93
p=0.007
p=0.009
p=0.001
p=0.88
p=0.007
CtsD (mat/pre)
Map1Lc3-II
Sqstm1
c
PepA DAPI
PepA+ spots per cell
P<0.0001
d
Oligo
FCCP
Rot+Ant
OCR (pmol/min/10^4 cells)
Time (min)
P=0.016
P=0.063
P=0.0009
P=0.016
P=0.073
P=0.0005
P=0.0006
P=0.141
P=0.0276
Basal respiration
ATP production
Maximal respiration
e
Mitochondrial ROS (fluorescence intensity)
P<0.0001
f
Ybx3 DAPI
% nuclear Ybx3
g
Gene targets/Gapdh
P<0.0001
P=0.03
P=0.02
P=0.028
P=0.005
Lrp2
Cdc20
Ccna2
Cdk1
h
Pcna DAPI
% nuclear Pcna
i
Number of cells (×10^6)
Time (days)
P=0.0007
P=0.0009
j
BSA DAPI
BSA+ spots per cell
P=0.9320

Figure 6

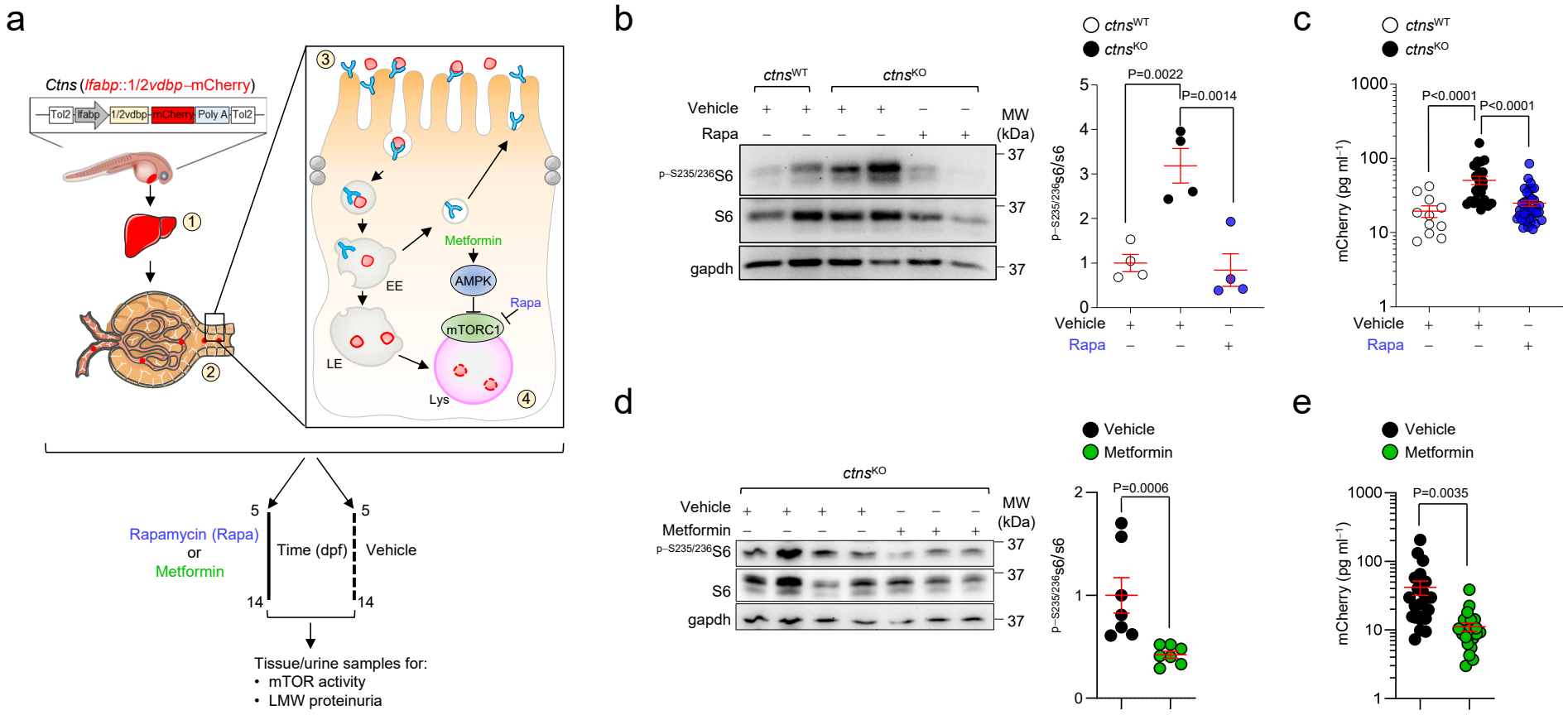
a
Ctns (lfabp::1/2vdbp–mCherry)
Tol2
lfabp
1/2vdbp
mCherry
Poly A
Tol2
Metformin
AMPK
Rapa
mTORC1
EE
LE
Lys
Rapamycin (Rapa)
or
Metformin
Time (dpf)
Vehicle
5
14
Tissue/urine samples for:
• mTOR activity
• LMW proteinuria
b
ctnsWT
ctnsKO
Vehicle
Rapa
MW (kDa)
p–S235/236S6
S6
gapdh
37
P=0.0022
P=0.0014
p–S235/236s6/s6
c
P<0.0001
P<0.0001
mCherry (pg ml−1)
d
Metformin
P=0.0006
e
P=0.0035